# Trajectory Surface Hopping Nonadiabatic Molecular Dynamics with Kohn–Sham ΔSCF for Condensed-Phase Systems

Mališ, Momir ; Luber, Sandra

Abstract: We present an efficient approach for surface hopping-based nonadiabatic dynamics in the condensed phase. For the systems studied, a restricted Kohn–Sham orbital formulation of the delta self-consistent field (ΔSCF) method was used for efficient calculation of excited electronic states. Time-dependent density functional theory (DFT) is applied to aid excited-state SCF convergence and provide guess electronic state densities. Aside from that the Landau–Zener procedure simplifies the surface hopping between electronic states. By utilizing the combined Gaussian and plane waves approach with periodic boundary conditions the method is easily applicable to full atomistic DFT simulations of condensed-phase systems and was used to study the nonradiative deactivation mechanism of photoexcited diimide in water solution.

DOI: https://doi.org/10.1021/acs.jctc.0c00372

# Trajectory Surface Hopping Nonadiabatic Molecular Dynamics with Kohn-Sham $\triangle$SCF for Condensed Phase Systems

Momir Mališ and Sandra Luber*

*University of Zurich, Department of Chemistry, Winterthurerstrasse 190, CH-8057 Zürich, Switzerland*

E-mail: sandra.luber@chem.uzh.ch

**Abstract**

We present an efficient approach for surface hopping-based nonadiabatic dynamics in the condensed phase. For the systems studied, a restricted Kohn-Sham orbital formulation of delta self-consistent field ($\Delta$SCF) method has been used for efficient calculation of excited electronic states. Time-dependent density functional theory is applied to aid excited state SCF convergence and provide guess electronic state densities. Aside from that the Landau-Zener procedure simplifies the surface hopping between electronic states. By utilizing the combined Gaussian and plane waves approach with periodic boundary conditions the method is easily applicable to full atomistic DFT simulations of condensed phase systems, and was used to study the nonradiative deactivation mechanism of photoexcited diimide in water solution.

## 1 Introduction

Nonadiabatic processes are ubiquitous in nature and the majority of them happens in the condensed phase. Whereas biologically light driven processes usually take place in the liquid

phase, artificial ones are also being developed in the solid phase. Simulating them, in order to better understand and optimize them, is a formidable theoretical and computational challenge. As the complexity grows exponentially with the system size, only semi-classical methods can cope with the difficulties, with the nonadiabatic molecular dynamics (NA-MD) at its forefront. NA-MD strongly depends on the electronic structure method used for description of excited electronic states. For condensed phase systems this is further made difficult by the number of closely interacting elements, the number of excited states, not to mention the possibility to treat the system periodically in order to include long range interactions effects. From the usual set of available tools to simulate such systems, the quantum mechanics (QM)/molecular mechanics (MM) approach represents a compromise, where an active part of the system is treated at QM level, while the rest is taken as an environment modeled at a lower level of theory, typically with force fields. A large variety of QM/MM approaches has been developed and used extensively, and we list just a few studies made with them.[1–8] QM/MM, however, becomes unpractical when the system cannot be clearly partitioned, a scenario usually encountered in modeling charge mobility in photovoltaic materials,[9] or the force fields are inadequate to capture the polarization effects for different electronic states.[10,11] The latter may be accounted for with polarizable continuum models,[12] particularly in cases where the nuclear dynamics is negligible,[13] but similar to QM/MM, the system requires a priory partitioning which is not always applicable. In these cases the all-atom and possibly periodic description at the same QM level becomes more appealing. Approximated electronic structure methods, e.g., semiempirical,[14] density functional tight-binding,[15–17] and fragmented molecular orbitals,[9,18,19] were applied for NA-MD on large (periodic) systems.

When it comes to accuracy, the choice of available electronic structure methods for condensed phase systems narrows down to the use of Kohn-Sham (KS) density functional theory (DFT) due to its good compromise between accuracy and computational efficiency. One possibility for excited electronic states is time-dependent (TD) DFT which has been previously

used for NA-MD with periodic boundary conditions.[20–22] The other option is the delta self-consistent field (ΔSCF) method, which instead of obtaining excited state properties from the perturbation of the ground electronic state density by solving the TD-DFT density response function,[23,24] constructs the excited electronic state with the variational principle, and calculates the required properties directly from it using the same ground state DFT subroutines.[25–29] Like the ground state, the excited state electronic densities are constructed from KS molecular orbitals whose occupation numbers are appropriately adjusted and also optimized in some ΔSCF variational procedures. Thus an excited state is available with the ΔSCF method at the same level and computational cost as the ground DFT electronic state. The method is easy to implement into existing DFT software packages, due to which it has been used for modeling excited states and their NA effects of bulk systems and surface bounded molecules.[27–32] Recent ΔSCF method assessments show that excited state energies match accurately with TD-DFT results over a wide configurational space including regions with conical intersections,[31,33–35] and the method is also less prone to problems of underestimated charge transfer states.[36] Like the ground DFT electronic state, a guess electronic density is required for the variational procedure, where some educated guess or other excited state method may be used to provide the initial starting excited state electronic density.

The other important aspect of NA-MD is the coupled electron-nuclear dynamics. While a number of different methodologies have been developed over the years (the reader is referred to review papers[37],[38] and[39] for more details), the trajectory surface hopping (TSH) approach stands out due to its simplicity and easily implemented procedure, which makes it also suitable for condensed phase simulations. TSH-NA-MD is a well established semi-classical methodology for describing the evolution of the system in the excited electronic states. For detailed derivation and explanations of the TSH-NA-MD, as well as its limitations, the reader is referred to the following references and the references within.[37,40–44] A commonly used procedure for switching between electronic states during TSH-NA-MD is the Tully's fewest-switch (FS) surface hopping (SH) algorithm.[45] Another option is the

Landau-Zener (LZ)[46–48] SH algorithm, particularly its adiabatic reformulation by Belyaev and Lebedev,[49] which was shown by Xie et al. to give the same results as the Tully's FS-SH for the systems studied.[50,51] This reformulation is particularly appealing since NA coupling terms are not required, while LZ generally avoids inclusion of decoherence corrections necessary with Tully's FS-SH algorithm.[52] The LZ algorithm was used by Tavernelli and coauthors for TSH-NA-MD in condensed phase systems described at the QM/MM level.[20,21]

Particularly interesting are the applications of the efficient ΔSCF method in excited states for ab initio NA-MD. Lin et al. were first to use the ΔSCF method for TSH-NA-MD of periodic systems enabling the whole system to be treated at the same DFT level.[53] These authors have simulated energy dissipation from excited electronic to phonon states in a periodic bilayer of $MoSe_2$ to model the light to heat conversion mechanism in solid photovoltaic materials.[53,54] The excited states were obtained by promoting a fixed number of electrons to the lowest virtual orbitals and by keeping their occupation fixed during ΔSCF. For the electronic structure calculations they have chosen the Vienna Ab initio Simulation Package[55] and coupled it with their in-house TSH procedure that later evolved into a QMXD code.[56] Similarly, Pradhan and coauthors have coupled the Quantum Espresso[57] program package with the Libra code from Akimov[58] using the ΔSCF method, and reported using it for examination of the nonradiative deactivation (NRD) mechanisms for few systems in gas phase.[35] In their ΔSCF implementation fractional occupations of spin-unrestricted KS orbitals have been used.

In this work we present NA-MD for the condensed phase using the CP2K software package[59] which is widely used for all-atom ab initio and DFT MD calculations of condensed phase systems.[60,61] For the systems studied in this work, we used the ΔSCF with restricted KS molecular orbitals and fixed occupation numbers for calculation of excited electronic states and their corresponding properties based on the mixed Gaussian and plane waves approach. Tamm-Dancoff linear response (LR) TD-DFT[62] was employed for the initial guess of excited state electronic densities. We applied Belyaev and Lebedev's reformulation of LZ-SH

for NA transitions between electronic states, although Tully's FS-SH is also possible with our implementation (see section 2 and Supporting Information). By using the LZ-SH we avoid the calculation of NA coupling terms at the ΔSCF level. To the best of our knowledge, we present here the first ΔSCF based TSH simulations conducted with the CP2K program package and application to periodic systems using LZ-SH.

We have applied our CP2K ΔSCF based TSH-NA-MD on two systems: ethylene in gas phase which we used to validate our implementation; and diimide molecule in water solution as a simple example of a condensed phase system. NRD pathways of the electronically excited $^1\pi\pi^*$ state of ethylene were thoroughly investigated in a number of previous studies.[35,63–72] The second system we studied is the diimide molecule, the simplest diazo compound. It is isoelectronic to ethylene, and like ethylene it has been used in a number of theoretical studies since its discovery.[73–80] While the isomerization reaction between its *trans* and *cis* conformers in the ground electronic state has been of great interest,[73,75,78–80] only a small number of studies have examined diimide's dynamics in the excited states. Tavernelli and coauthors have simulated a few trajectories in gas phase for both conformers initiated in the first singlet excited state, and examined the influence of initial conditions and the use of a thermostat in their NA-MD simulations on the diimide NRD mechanism.[81] Handt et al. have used their developed semiclassical NA equation-of-motion methodology to study the photodynamics of isolated diimide whose photoabsorption process was also explicitly simulated.[82] In both studies TD-DFT based methods were used for construction of electronic states. On the experimental side, lifetime measurements and characterization of photoproducts have been made for the photoexcited diimide in gas phase,[83–85] but there are no time-resolved investigations of the deactivation mechanisms. As for the condensed phase, only an absorption spectrum of diimide in aqueous solution was reported up-to-date.[86] On the other hand, the excited state dynamics of diimide's methylated analogue ($H_3C$–N=N–$CH_3$) has been studied experimentally and theoretically in gas phase and solution.[87–96] In order to fill the gap we conducted NA-MD on a diimide molecule solvated in a periodic box of water molecules in

order to model the liquid state in a sound manner. This also allowed us to investigate the potential effects of explicit solvent molecules on diimide's NRD mechanisms.

The paper is structured as follow: section 2 gives a very brief overview of TSH and a detailed description of our ΔSCF method with CP2K; After the computational methods in section 3, section 4 reports the findings of NA-MD simulations conducted on ethylene and diimide systems, respectively, while the final conclusions are given in section 5.

# 2 Theory

The TSH-NA-MD is based on approximating the exact quantum nuclear wave packet evolution with a number of classical trajectories that are propagated in a manifold of adiabatic electronic states. For details, we refer to Refs.[37,40–44]. Using $E_i(\mathbf{R}_t)$, the adiabatic energy of the $i$-th electronic state, which is an eigenvalue of the electronic Hamiltonian $\hat{H}_e$ at a nuclear configuration $\mathbf{R}_t$,

$$\hat{H}_e(\mathbf{R}_t)\,|\psi_i(\mathbf{R}_t)\rangle = E_i(\mathbf{R}_t)\,|\psi_i(\mathbf{R}_t)\rangle\,, \tag{1}$$

a linear combination of orthogonal adiabatic electronic eigenfunctions $|\psi_i(\mathbf{R}_t)\rangle$ of Eq. (1) within the manifold of electronic states describes the system's total electronic wave function

$$|\Psi(\mathbf{R}_t)\rangle = \sum_i \phi_i(\mathbf{R}_t)\,|\psi_i(\mathbf{R}_t)\rangle\,. \tag{2}$$

$\phi_i(\mathbf{R}_t)$ designates the corresponding coefficients whose evolution along the trajectory is given by the time-dependent (TD) Schrödinger equation (SE)

$$\imath\hbar\frac{d\phi_i(\mathbf{R}_t)}{dt} = E_i(\mathbf{R}_t)\phi_i(\mathbf{R}_t) - \imath\hbar\sum_{j\neq i}\phi_j(\mathbf{R}_t)\,\langle\psi_i(\mathbf{R}_t)|\,\nabla\,|\psi_j(\mathbf{R}_t)\rangle\cdot\frac{d\mathbf{R}_t}{dt}, \tag{3}$$

and whose square of the absolute value gives the $i$-th electronic state population number $P_i$ $(=\phi_i^*\phi_i)$. The NA coupling vectors $\langle\psi_i|\,\nabla\,|\psi_j\rangle$ in Eq. (3) induce the population transfer

between the $i$-th and $j$-th pair of electronic states. From aforementioned, it is clear that, among others, the quality of electronic states, namely the corresponding energies, gradients and NA coupling elements, together with the trajectory's initial conditions and simulation length determine the outcome of NA-MD simulations. For the condensed phase, the determination of excited states, and their properties, is particularly computationally expensive, so simulations are usually done in the framework of DFT.

In this work, we use the ΔSCF method[25–29] for the calculation of excited electronic states and their gradients. ΔSCF is based on the existence of an excited electronic state density $\rho_i(\vec{r})$ for each excited electronic eigenstate $|\psi_i\rangle$, which in the limit of the adiabatic approximation is described by stationary KS DFT.[33] In terms of DFT KS molecular orbitals $\varphi^i_{j\sigma}(\vec{r})$ the total electronic density of the $i$-th electronic state is

$$\rho_i(\vec{r}) = \sum_{\substack{j \\ \sigma=\{\alpha,\beta\}}} n^i_{j\sigma} |\varphi^i_{j\sigma}(\vec{r})|^2 = \rho^\alpha_i(\vec{r}) + \rho^\beta_i(\vec{r}), \tag{4}$$

where $n^i_{j\sigma}$ are the occupations of the $j$-th KS orbital with spin state $\sigma$. $\vec{r}$ is a three-dimensional position vector. The total density (4) is the sum of the two spin densities, $\rho^\alpha_i(\vec{r})$ and $\rho^\beta_i(\vec{r})$. Orbital occupations numbers can be fractional but must satisfy $\sum_{j,\sigma} n^i_{j\sigma} = N_e$, where $N_e$ is the total number of electrons. The KS molecular orbitals are eigenfunctions of the KS equation

$$\left( -\frac{\hbar^2}{2}\nabla^2 + w(\vec{r}) + \int \frac{\rho_i(\vec{r}')}{|\vec{r} - \vec{r}'|}\, d\vec{r}' + v_{\mathrm{xc}}[\rho^\alpha_i, \rho^\beta_i](\vec{r}) \right) \varphi^i_{j\sigma}(\vec{r}) = \epsilon^i_j \varphi^i_{j\sigma}(\vec{r}). \tag{5}$$

The first term on the left-hand side (l.h.s.) parenthesis of Eq. (5) is the kinetic energy operator for noninteracting electrons, while the three remaining terms are the external electrostatic (including electron-nuclei interaction), electron-electron repulsion (including electron self-interaction), and exchange–correlation potentials, respectively. Because of the functional dependence of the latter two terms on the total system electronic density and the difference

of the two spin densities, the eigenpair solution of Eq. (5) is obtained in a self-consistent procedure. Ideally, the exchange–correlation functional should correct for all the effects the KS noninteracting density structure omits, but in reality it only corrects them to a certain level. Similarly to DFT with fractionally occupied KS orbitals,[97] the corresponding total electronic energy of a state with electronic density $\rho_i$ is given by the expression

$$E_i = -\frac{\hbar^2}{2} \sum_{\substack{j=1 \\ \sigma=\{\alpha,\beta\}}} n^i_{j\sigma} \left\langle \varphi^i_{j\sigma} \right| \nabla^2 \left| \varphi^i_{j\sigma} \right\rangle + \int \left( w(\vec{r}) + \frac{1}{2} \int \frac{\rho_i(\vec{r}')}{|\vec{r} - \vec{r}'|} \, d\vec{r}' + v_{\mathrm{xc}}[\rho^\alpha_i, \rho^\beta_i](\vec{r}) \right) \rho_i(\vec{r}) \, d\vec{r}. \tag{6}$$

The corresponding ground state electronic density has the lowest energy KS orbitals populated according to the Aufbau principle with occupation numbers $n_{i,\sigma}$ equal to one, while zero for the other remaining KS orbitals. This density can be represented as a Slater determinant composed of KS orbitals. DFT with fractionally occupied KS orbitals optimizes also the orbital occupation numbers in addition to KS orbitals to get the lowest electronic energy.[98] Care should be taken into account because the Hohenberg-Kohn theorem does not hold for excited states, and the presence of a local minimum does not necessary guarantee a meaningful excited state density.[33,99]

But the main challenge is the excited state density itself since ΔSCF cannot directly give an excited electronic state density, nor even guess one. Instead the initial density, i.e. occupation numbers, has to be provided a priori, either by an educated guess, or by using a suitable electronic structure method. We use Tamm-Dancoff LR-TD-DFT within CP2K[62] to provide the initial excited electronic state density, as well as a reference to compare the ΔSCF results to. It should be noted that, contrary to the ΔSCF method, the LR-TD-DFT does not directly construct the electronic excited state densities but instead gives the characteristic electronic density change relative to the ground state electronic density of a system perturbed by a weak external field. Therefore, the corresponding LR-TD-DFT density change has to be combined with the ground state electronic density in order to reconstruct the excited state electronic density. Within LR-TD-DFT in the Tamm-Dancoff approximation the electronic

density change is expressed as a linear combination of occupied ($o$) and unoccupied ($u$) ground state KS orbital pairs, $\varphi_{o\sigma}(\vec{r})\varphi_{u\sigma}(\vec{r})$, weighted with corresponding coefficients $X^i_{ou\sigma}$ for each electronic state $i$. The latter are the elements of the eigenvector of Casida's equation in the Tamm-Dancoff approximation for the $i$-th excited electronic state.[100] Since the sum of squares of coefficients over all unoccupied KS orbitals for a particular ground electronic state occupied orbital ($\sum_u |X^i_{ou\sigma}|^2$) gives the change of its occupation number, the corresponding occupation number in Eq. (4) for the occupied KS orbital of the $i$-th electronic excited state is $n^0_{o\sigma} - \sum_u |X^i_{ou\sigma}|^2$, where $n^0_{o\sigma}$ is the corresponding occupation number of the ground electronic state. Analogously, the occupation number of a KS orbital, that was unoccupied in the ground electronic state, in the $i$-th electronic state is $\sum_o |X^i_{ou\sigma}|^2$. This gives our guess electronic density for the $i$-th excited electronic state.

Converging the ΔSCF states can also been challenging. The excited state energy (6) is minimized by optimizing the KS orbitals and their occupations with a restrain that the electronic density resembles the excited state electronic density. The occupation numbers are typically kept fixed and changed by small amounts only when KS orbital optimization exhibits convergence issues. Previous ΔSCF procedures used for ab initio MD report updating the fractional occupations either by Gaussian smearing,[6] or smearing with the Fermi-Dirac distribution function.[35] In our ΔSCF procedure, we update orbital occupation numbers with TD-DFT as explained previously. As we are also fixing the orbital occupations and optimizing only the KS orbitals, we have constructed an elaborated SCF convergence scheme consisting of several consecutive SCF diagonalization algorithm changes in order to converge the ground and excited electronic states (see Fig. 1). In case the SCF convergence fails, a TD-DFT calculation is conducted to construct the new occupation numbers and the SCF is repeated. After convergence is achieved, the occupation numbers are rounded to the nearest integers and SCF repeated once more. This assures that the excited electronic states are constructed consistently by using the same occupation numbers, and minimizes the use of TD-DFT calculations in subsequent trajectory steps. The TD-DFT calculation also provides

a new reference excited state density and checks the nature of excited electronic states. This is important in case of appearance of any new state along the NA-MD. Reusing the KS orbitals from the previous trajectory step also speeds up the SCF convergence. TD-DFT calculations are also called in the first trajectory steps.

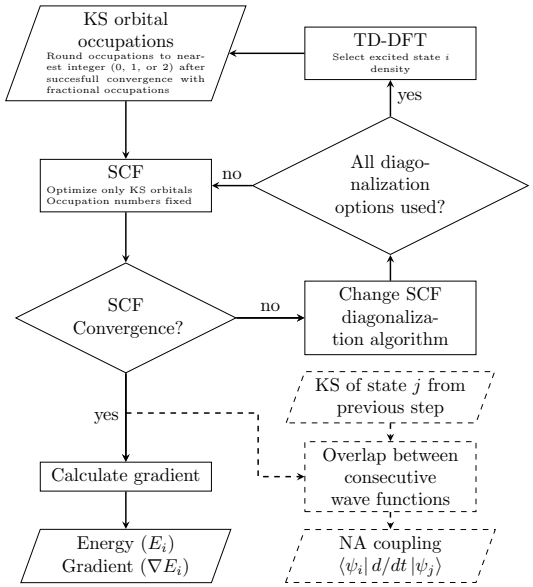


Figure 1: Scheme of the ΔSCF procedure for obtaining the excited state energy and gradient. Converged KS orbitals can be optionally further used to calculate the NA coupling terms (indicated with dashed lines). For more information see the Supporting Information.

Another difference with our ΔSCF scheme compared to the ones used in Refs.[6] and[35] is that we use restricted instead of unrestricted KS orbitals for the treatment of singlet excited electronic states in order to avoid spin contamination. In other words, spatial KS orbitals for the alpha and beta spin channels are identical ($\varphi_{i\alpha} = \varphi_{i\beta}$) and, because the occupation number is equally shared between the two spins, the difference between the $\alpha$ and $\beta$ spin densities is zero, as expected in the singled excited electronic state. The use of restricted KS orbitals in ΔSCF reminds of the restricted-open (RO) KS[101] and the RO singlet state (SS)[102,103] formulations, which also have identical spatial KS orbitals for the two spin channels. However, the latter two methods construct the excited singlet state energy indirectly from energies belonging two identical total densities but both with individually different spin densities through the use of a spin purification formula.[25] Both of these two

electronic densities have a different contribution to the exchange–correlation term $v_{\mathrm{xc}}[\rho_i^{\alpha}, \rho_i^{\beta}]$ but none reproduces the proper contribution of the singlet state directly. The SCF procedure has to converge the two distinct electronic densities, either simultaneously like in the RO-KS and RO-SS methods,[104,105] or independently as typically performed with unrestricted ΔSCF.[106] The latter is particularly impractical for NA-MD while it requires two independent SCF calculations instead of one, and, apart from the singlet state electronic energy, does not provide directly any other excited state property[101] nor a clear procedure for determining NA couplings like with the RO-KS method.[107] The use of restricted KS orbitals with equally split occupation numbers between the two spin channels simplifies the ΔSCF procedure as it converges only one density. In fact, because of the imposed symmetry between the two spin channels, they are combined, yielding only one set of KS orbitals whose occupation numbers range from 0 to 2, where those in between we further round to the nearest integer. This is the same formulation as previously used in a number of spin-unpolarized restricted KS ΔSCF methods.[30,31,108] The exchange–correlation term is provided with an excited state electronic density that has no difference in spin densities and resembles more the singlet exited state. Note that within DFT it is not possible to uniquely distinguish whether such an electronic density belongs to a singlet excited, or a triplet excited state with zero projection of the total spin ($S = 1$, $S_z = 0$). However, since there is no difference between spin densities it is certainly not a superposition of these two states, and all our calculations show that the corresponding electronic energy is similar or higher than the RO-KS singlet state energy. The use of restricted KS orbitals limits the application of this ΔSCF approach only to closed shell systems and singlet excited states. Once the ΔSCF energy (6) is converged, the corresponding KS orbitals and occupation numbers are inserted into the ground state DFT gradient subroutine to obtain the excited electronic state gradient.

Because ΔSCF excited electronic states behave diabatically and are mutually independent, they are reordered according to their electronic energy at every trajectory step. As for the NA coupling elements between electronic states, they can only be approximated since

ΔSCF per se does not give a sound insight into electronic wave functions. The direct overlap of nonorthogonal Slater determinants transforms the TD-SE (3) to

$$\sum_i S_{ji}(\mathbf{R}_t)\frac{d\phi_i(\mathbf{R}_t)}{dt} = \sum_i \left\{ -\frac{\imath}{\hbar}\left\langle\psi_j(\mathbf{R}_t)\right| \hat{H}_e(\mathbf{R}_t) \left|\psi_i(\mathbf{R}_t)\right\rangle - \left\langle\psi_j(\mathbf{R}_t)\right| \frac{d}{dt} \left|\psi_i(\mathbf{R}_t)\right\rangle \right\}\phi_i(\mathbf{R}_t). \tag{7}$$

The full derivation of Tully's FS-SH in restricted KS ΔSCF, discussion of arising complications and our implementation are given in the Supporting Information. We also investigated the hermitian coupling term (see Eq. S11) arising from the nonorthogonality in comparison to the antihermitian terms standardly used. Interestingly, for the examples studied neglecting the hermitian term gave smoother NA couplings between the ground and excited electronic state which for the examined system were similar to the TD-DFT NA coupling values obtained from the auxiliary wave functions (see the comparison in Supporting Information). We included this option of computing the NA couplings into our implementation (details in the Supporting Information), but for the studied systems we use the LZ formula rewritten in adiabatic representation,[49] for which the probability of hopping from electronic state $i$ to $j$ is

$$\mathcal{P}_{i\to j} = \exp\left(-\frac{\pi}{2\hbar}\sqrt{\frac{Z_{ij}^3}{\ddot{Z}_{ij}}}\right), \tag{8}$$

where $Z_{ij} = |E_i - E_j|$ is the potential energy gap between the two electronic states, while the double dot indicates second order derivation with respect to time. This last term is evaluated numerically from energy differences of the three last points along the trajectory as in Ref.[51]. Unlike the original Tully's FS-SH algorithm[45] LZ does not require additional procedures to account for the missing decoherence.[52] With the LZ the use of the NA couplings can be eliminated altogether as well as the propagation of electronic populations in Eq. (3). Note that the population of electronic state $P_i$ in the LZ-SH formulation is given by the ratio of the current number $N_i$ of trajectories being evolved in the electronic state $i$ to the total number of trajectories $N_{\text{traj.}}$, $P_i(t) = N_i(t)/N_{\text{traj.}}$.

# 3 Computational Details

The CP2K code was coupled to the Zagreb Surface Hopping NA-MD code developed by the Došlić group and available through the E-CAM software repository.[109–111] Nuclear trajectories were propagated with the velocity Verlet algorithm. If the LZ-SH probability for a hop to another state, calculated for each trajectory step, is larger than a random uniform number $\xi \in [0, 1]$, the NA hop takes place. The nuclear velocities are then rescaled along the direction of the gradient difference between the new and previous electronic states in order to conserve the total energy.[112] Hops which violate energy conservation are discarded and the trajectory continues in the current electronic state.

For NA-MD, the initial conditions for the systems in gas phase were sampled from a thermalized Wigner distribution function while for the condensed phase from ab initio MD. Details for each are given in the Supporting Information.

All NA-MD simulations were conducted using the PBE0 functional[113] with the auxiliary density matrix method (ADMM)[114] and the TZVP-GTH basis set[115] with Goedecker-Teter-Hutter (GTH) pseudopotentials[116], while the plane wave cutoff was set to 500 Ry. Empirical dispersion corrections of the D3 type[117] were included in the condensed phase calculations. A nuclear propagation time step of 0.5 fs was used for the NA-MD runs. All NA-MD trajectories were evolved in a microcanonical (NVE) ensemble. The CP2K code was used for all electronic structure calculations, unless stated otherwise. For our restricted KS $\Delta$SCF calculations the occupations of corresponding KS orbitals were adjusted by providing an occupation list, in case of RO-KS calculations by manually alternating the occupations for the two spin channels within the SCF part of the code. Turbomole 7.3[118] was employed for the calculations of excited electronic states at the algebraic diagrammatic construction scheme of the second order (ADC(2)) level[119,120] which were compared to the energies and nature of $\Delta$SCF and TD-DFT excited electronic states. Gaussian 09[121] was used for the CASSCF calculations. The same TZVP basis set by Schäfer et al.[122] was used with the latter two codes.

# 4 Results and Discussion

## 4.1 Benchmarking Restricted KS ΔSCF Energies for Ethylene and Diimide

We first compare the energies obtained at the restricted KS ΔSCF level for the two systems of interest with few selected methods. Electronic energies were determined along a simplified *cis* to *trans* isomerization pathway described by the torsional angle of the systems' double bonds (see Fig. 2b). All other geometric parameters were fixed to values corresponding to their minimum energy structures in the ground electronic state at the PBE0/TZVP level. Figure 2a depicts the energy profile of the ground electronic and the two lowest singlet excited electronic states on the torsional angle between the $CH_2$ groups in ethylene calculated at the ADC(2), TD-DFT, and ΔSCF levels of theory. At the ΔSCF level the first singlet excited state, also called the V state, is 7.12 eV above the minimum geometry ground electronic state (N state) energy and corresponds to $\pi\pi^*$ character. The same excitation calculated at the Tamm-Dancoff LR-TD-DFT level is slightly higher, 7.78 eV, while the ADC(2) result is 8.40 eV. The entire torsional potential energy curve calculated at the ΔSCF level using the hybrid PBE0 functional and the Gaussian and plane waves approach is shifted by about 1.3 eV above the potential energy curve previously obtained by Pradhan at el., which used the unrestricted ΔSCF method with a PBE functional and a plane waves code.[35] This shift alleviates the negative energy difference between the V and N electronic states which the same authors have obtained with the PBE functional at angles close to 90°.[35] It is worth mentioning that a very good agreement with the singlet excited electronic state energies calculated with the RO-KS method was obtained. The calculated ΔSCF vertical excitation compares well to the experimentally reported $\pi\pi^*$ electronic excitation reported at ∼6.2 eV[123–125] and at 7.7 eV[126,127].

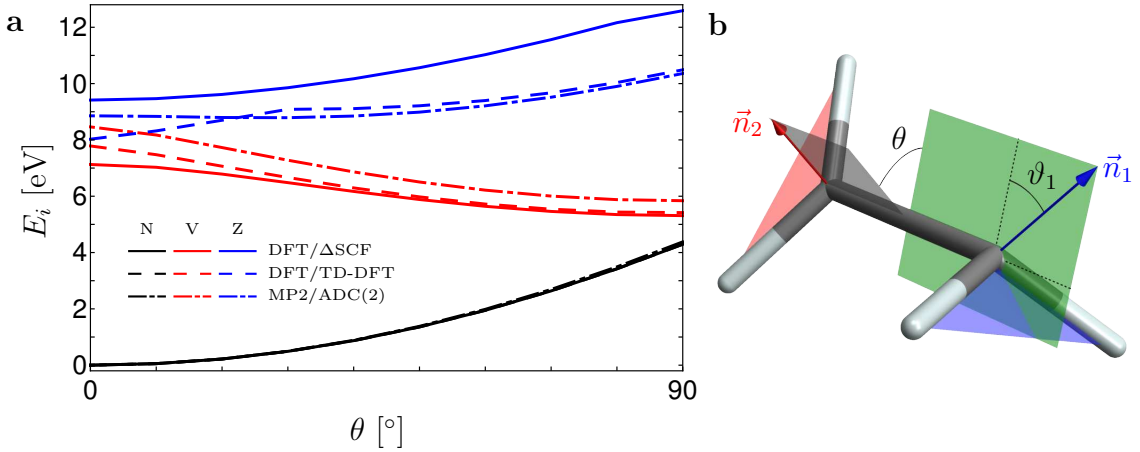


Figure 2: a) Energies of the N (black line), V (red) and second singlet excited (blue) states relative to the N state minimum geometry energy as a function of the torsional angle between the $CH_2$ groups in ethylene. All other ethylene geometric parameters were kept at the N electronic state equilibrium geometry values. Solid, dashed, and dotted-dashed lines show energies calculated at the ΔSCF, Tamm-Dancoff TD-DFT, and ADC(2) methods, respectively. For all calculations, only the torsional angle was varied, while all other ethylene geometry parameters were kept at N state minimum geometry values. b) Definition of the pyramidalization angle ($\vartheta$) and torsional angle ($\theta$) in ethylene. Two C–H bonds of the same $CH_2$ group define a plane (blue) with a normal vector ($\vec{n}_1$). With the direction of the C–C bond it defines a torsional plane (green) for the first $CH_2$ group. The angle between the two torsional planes of each $CH_2$ group defines the torsional angle $\theta$. Pyramidalization angle $\vartheta$ is the inclination of the normal $\vec{n}$ from the direction orthogonal to the C–C bond and laying in the corresponding torsional plane. At the ethylene ground state equilibrium geometry all angles are zero.

At all three examined levels of theory, the calculated V states are of the same nature, corresponding to the electronic density reduction in the C=C region, while in terms of molecular orbitals (KS orbitals at the DFT level) all have the HOMO to LUMO transfer as their most dominant contribution. The reduction of the electron density in the V state makes the torsion of the C=C bond energetically favorable. As for the N state, any torsion of the double bond destabilizes the N electronic state, rising its energy up by 4.29 eV for the 90° torsion angle. The energy gap at the ΔSCF level between the V and N states at this geometry is 1.02 eV, while 2.6 eV at the MR-CISD/SA-3-CAS(2,2)/aug-cc-VDZ level.[66] This is due to the missing multireference character of the N state which single reference methods typically cannot reproduce at these geometries.[66,128] For the same reason the N state curve

exhibits a cusp at 90° instead of the smooth transition.[128–130]

The second excited electronic state the single reference methods give (blue lines in Fig. 2) is the $\pi 3s$ Rydberg state. It is highly overestimated compared to reported values (see for example in Refs.[70,71]) because the used TZVP basis set lacks diffusive orbitals, but properly increases in energy with respect to the increase of the torsional angle. Because a number of recent studies had demonstrated the role of the Rydberg states in the initial phase of ethylene NA-MD with ambiguous conclusions on the overall excited state lifetime,[70–72] we do not include Rydberg states in the manifold of excited states but keep in mind their potential effects. Single reference methods fail to reproduce the nature of the second non-Rydberg excited electronic state (called the Z state), which is of the double excitation character ($^1\pi_2^*$) and whose electronic energy decreases with the torsional angle and intersects the V state at angles close to 90°.[64,66,70,131,132] The potential energy curve of the Z state, obtained by the ΔSCF method, qualitatively agrees with multireferences methods. Converging this state at the ΔSCF level, however, proved to be an issue as the SCF convergence scheme failed for torsional angles larger than 60°.

Diimide's lowest singlet excited states are similar to those of ethylene. The first singlet excited state is of $n\pi^*$ character,[74,76] which has a weakened N=N bond due to the population of the $\pi^*$ orbital. Figure 3 shows the energy of the ground and first excited electronic states on the torsional angle between the two NH groups. As in case of ethylene, single reference methods fail to properly describe the ground electronic state at angles close to 90° by overestimating the ground state barrier and displaying a cusp at the 90° angle, which are particularly exhibited at the MP2 level.[133] On the other hand, the TD-DFT and the ADC(2) methods underestimate the energy of the first excited state. For a better comparison with the multireference methods, energy curves at the SA-CASSCF(6,4)/TZVP level are also shown (see Supporting Information for more details). The ΔSCF curve is systematically shifted by an almost constant value of $1.35 \pm 0.04$ eV and $0.93 \pm 0.05$ eV from the TD-DFT and ADC(2) values, respectively. It is also shifted relative to the energies of the

singlet excited state computed with the RO-KS method, which are similar to the TD-DFT results and also intersect with the ground electronic state. ΔSCF energies obtained with the B3LYP functional match up the PBE0 values, while omitting any exact Hartree-Fock exchange lowers the excited state slightly below the displayed TD-DFT energy curve, but above the RO-KS singlet state energy curve also computed without the exact Hartree-Fock exchange (not shown). The ΔSCF first excited state curve also indicates the presence of a local minimum similar to the one reported by Tavernelli et al. at the TD-DFT level.[81] The optimized excited state minimum and the conical intersection (CI) geometry between the two states at the SA-CASSCF(6,4)/TZVP level are given in the Supporting Information. In case of diimide the Rydberg states are higher in energy,[74] while the double excitation character of the second excited state displays the same issue as in case of ethylene.[133,134]

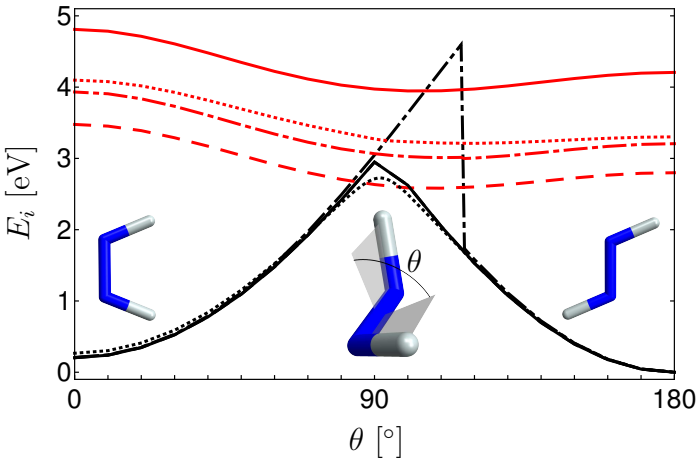


Figure 3: Energies of the ground (black line) and first singlet excited (red line) electronic states in diimide as functions of the torsional angle between the two NH groups. Solid, dashed, dotted-dashed and dotted lines show energies calculated at the ΔSCF, Tamm-Dancoff TD-DFT, ADC(2), and SA-CASSCF(6,4) methods, respectively. The *cis* isomer is indicated with the angle of 0°. The scan was made by varying only the HN=NH torsional angle starting from the minimum *cis* conformation. Energies are relative to the corresponding electronic ground state value of the *trans* conformer. The insets on the left and right show *cis* and *trans* diimide conformers, respectively, while the inset in the middle shows the definition of the torsional angle $\theta$.

Overall, the restricted ΔSCF method gives the lowest singlet excited states for ethylene that matches well with other single reference method results, while in case of diimide it

alleviates the issue of state intersection at distorted geometries, but preserves the underlying issues of the single reference methods. Thus, we included only the ground and first singlet excited electronic states into the NA-MD simulations.

## 4.2 NA-MD in Gas Phase

### 4.2.1 Ethylene

Figure 4 shows an evolution of N and V state electronic energies together with the most relevant geometrical parameters in one ethylene trajectory. This selected trajectory shows a typical behavior observed in the whole ensemble of studied trajectories. 400 trajectories in total were used to examine the NRD pathways of ethylene initiated from the V excited state in the Franck-Condon region of the configuration space. Each trajectory was propagated for 500 time steps. In the initial phase of the displayed trajectory a concerted motion composed of the C=C bond extension, the C=C bond torsion, and the pyramidalization of both $CH_2$ groups reduces the energy gap between the two states. At the 52.5 fs time mark the gap is only 0.03 eV and a NA hop to the N state occurs. Within the examined ensemble, all of the trajectories deactivate to the N state through similar twisted-pyramidalized CI geometries.[63] Once in the N state, all of the electronic energy is converted into vibrational motion. For the trajectory in figure 4 the energy is mostly transferred to the C–H bond vibrations and $CH_2$ groups pyramidalization vibrations, as observed from their amplitude increase. The torsional oscillation continues, but in this case it is insufficiently excited to cause the *cis-trans* isomerization. About half of the trajectories exhibit the *cis-trans* isomerization within the propagation time, while only a few show the hydrogen atom migration and forming of the ethylidene in the N state. We have observed only one trajectory that underwent a $H_2$ molecule ejection in the N state, leaving a vibrationally excited acetylene fragment behind.

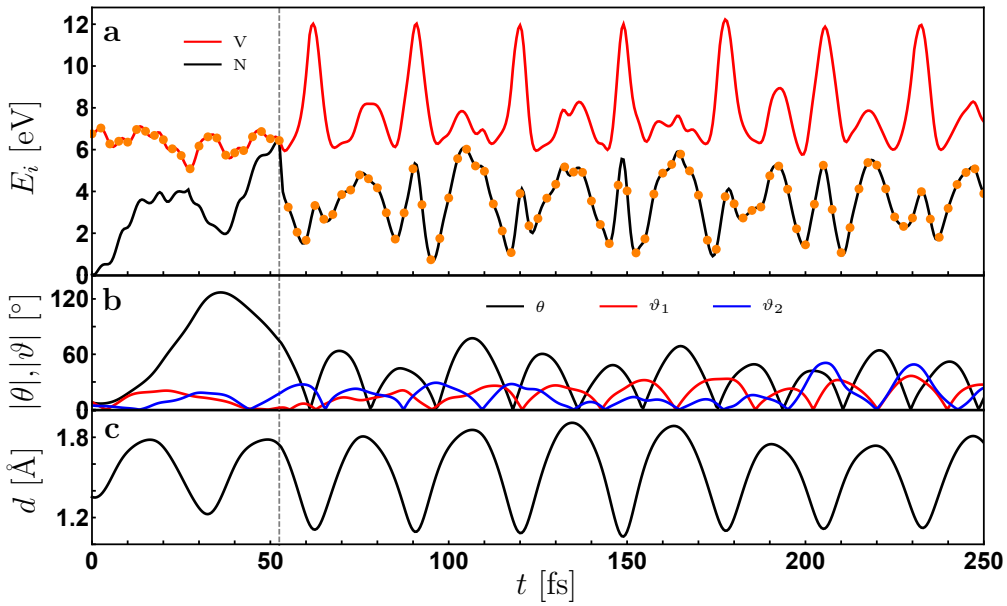


Figure 4: a) Evolution of the N (black) and V (red) state energies along a selected ethylene trajectory. The currently occupied state is indicated with orange points. A vertical gray dashed line indicates the moment a NA hop from the V to N state has occurred. All energies are relative to the smallest energy value along the whole trajectory. b) Evolution of the absolute torsional angle $\theta$ between the two $CH_2$ groups (black line) and the pyramidalization angles ($\vartheta$) for each $CH_2$ group (red and blue lines, respectively) of the same trajectory. For the angle definitions, see figure 2b. c) Evolution of the C–C distance ($d$) for the same trajectory.

We found a monoexponential decay function to fit the average population of the V state, see figure 5. The fitted lifetime of the V state is 33 fs, which is very close the two experimentally measured values, $30 \pm 15$ fs[123] and $20 \pm 10$ fs[124]. Note that according to Ref.[124], those experimental values should be interpreted as the time the nuclear wave packet requires to leave the Franck-Condon region and not the V state lifetime. Comparable studies applying a higher level of theory and quantum like NA methods report lifetimes of about 100 fs.[65,69–71] The vast methodological differences make a direct comparison not expedient. On the other hand, Pradhan and co-authors used an analogous $\Delta$SCF approach and reported a lifetime of 58 fs,[35] which is in reasonable agreement with our simulation. Few reasons might explain the difference to these previously published works. The first is the reduced energy gap between the excited and ground electronic states for the 90° twisted structures compared to more

accurate ab initio values,[66] which effects the LZ hopping probability by giving more frequent hops to the ground state. Although the gap is negative on the PBE-ΔSCF surface of Pradhan et al.,[35] they mitigated this issue by employing Tully's SH formula which is immune to erroneous negative energy differences at CI geometries. However, we are unaware how their nonadiabatic $\langle\psi_{\mathrm{V}}|\, d/dt\, |\psi_{\mathrm{N}}\rangle$ couplings compare to values obtained with other methods. Another contributing factor to the shorter lifetime, particularly to the previous ΔSCF value, is the use of initial conditions with significantly more kinetic energy, as ours were obtained by sampling from the Wigner, while theirs from the Boltzmann distribution function. This is in line with observation that the first distribution gives shorter lifetimes.[135] We also expect that the inclusion of other excited electronic states, mostly the second excited singlet state, as well as the Rydberg states, would, as reported,[71] temporarily trap the excited state population and prolong the V state lifetime.

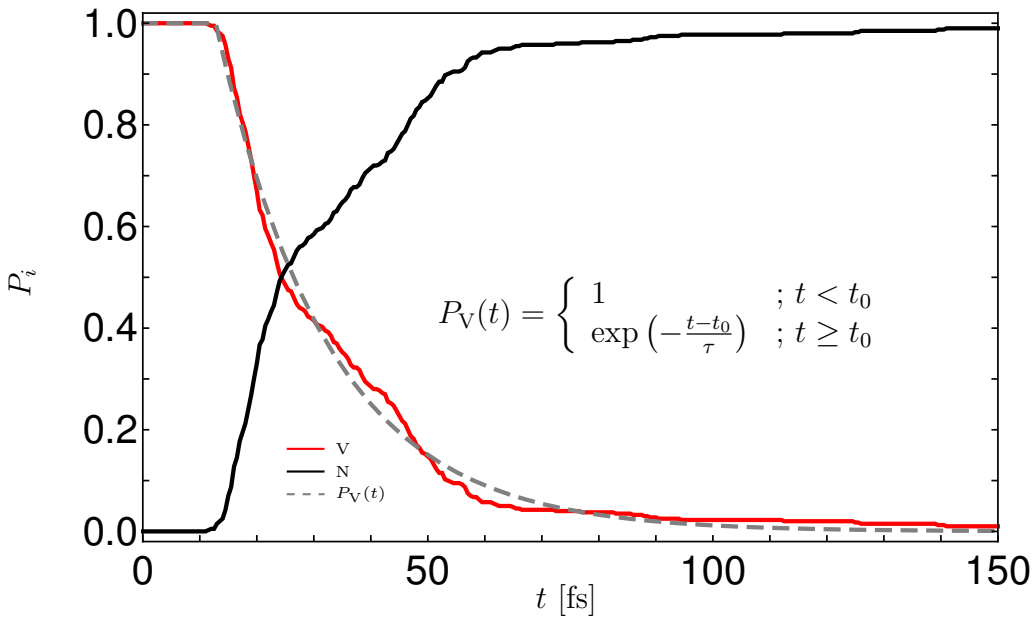


Figure 5: Evolution of the average population of the V (red line) and N (black line) states of the ensemble of 400 ethylene trajectories initiated from the V state. The dashed gray curve indicates the fitted decay function of the V state defined in the inset. Fitted values are $t_0 = 13$ fs and $\tau = 20$ fs, giving a lifetime $(t_0 + \tau)$ of 33 fs. Of the two fitted parameters, $t_0$ designates the onset of population transfer, while $\tau$ a exponential decay constant.

### 4.2.2 Diimide

A set of 100 trajectories for *trans*-diimide and a set of same size for the *cis*-diimide conformer in gas phase were propagated for 250 fs of the NA-MD. These two sets show similar behavior so the explanation is given only on the *trans*-diimide results and figures related to *cis*-diimide conformer are in the Supporting Information. Figure 6 displays results for all trajectories of the *trans*-diimide set. Dynamics resembles that of ethylene, with N=N bond extension and the two NH groups twisting along the N=N bond in the initial phase. This is the motion driving the system towards the excited electronic state minimum. For 83% of trajectories the energy difference between the two electronic states reaches or fells below 1 eV in the first 50 fs of NA-MD (see figure 6a). About 60% of trajectories ends in the ground electronic state within this period, while the remaining deactivates at a lower rate as the decay is biexponential (see figure 6b), with lifetimes of 37 and 153 fs. For the *cis* conformer they are 32 and 148 fs. Spikes in the energy differences are observed because of aforementioned insufficiency of ground state DFT at geometries distorted around 90°. These are the main cause for splitting of the population into deactivating channels of two different rates, because as the energy difference incorrectly decreases, the LZ algorithm detects a requirement for NA hop. Nonetheless, the NA hop happens in a region of configuration space with strong NA coupling between the two states. Thus, the smaller lifetime value can be regarded as a lower estimate of the diimide first excited state lifetime in a limit of a very strong NA coupling between the two states.

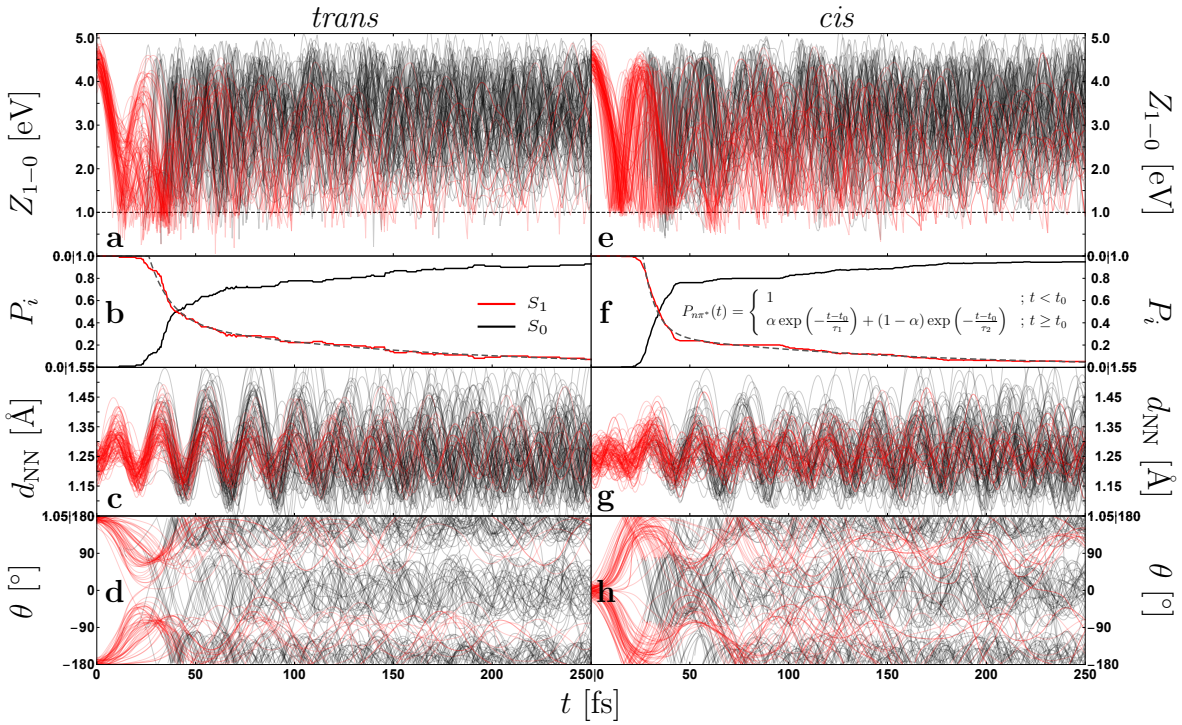


Figure 6: Evolution of 100 NA-MD trajectories for *trans*-diimide (left) and *cis*-diimide (right) in the gas phase. a) and e) Energy difference between the first excited and ground electronic states. b) and f) Average population of the first excited (red) and ground (black) electronic states. The fitted biexponential decay function for the first excited state is shown with a gray dashed line. The fitted decay function is shown in the inset of figure f. c) and g) N=N bond lengths for the same trajectories. d) and h) The torsional angle $\theta$ between the two NH groups along each trajectory. Lines in figures a, c, d, e, g and h are colored red (black) if the corresponding trajectory is in the first excited (ground) electronic state. The two obtained lifetimes for the *trans*-diimide are $t_0 + \tau_1 = 37$ fs and $t_0 + \tau_2 = 152$ fs, with $t_0 = 26$ fs, while the fraction of the trajectories deactivating via a shorter lifetime pathway ($\alpha$) is 0.59. The corresponding values for the *cis*-diimide are: $t_0 + \tau_1 = 32$ fs, $t_0 + \tau_2 = 148$ fs and $\alpha = 0.70$.

In order to further facilitate this point we shifted the first ΔSCF excited state relative to the ground electronic state by −1.0 eV. This brings the two DFT/ΔSCF potential energy curves in figure 3 almost in contact at the torsional angle of 90°, which causes a significant reduction in lifetime, because almost all trajectories deactivate to the ground state. The fitted lifetime of the first excited state in that case is 20 fs (see Fig. S5 in the Supporting Information), which is in line with the NA quantum molecular dynamics simulations of Handt and coworkers at the LDA/cc-pVDZ level of theory who observed that the nonadiabatic transition occurs ca. 20 fs after excitation.[82] When a switch to the ground state occurs, all of

the initially absorbed photon's ∼4 eV of energy is converted into internal vibrational energy, further increasing the amplitudes of diimide internal bond oscillations. Since a restricted KS formalism is used to obtain the ground and excited electronic state energies, no observation of diimide fragmentation is observed for the duration of the simulation. However, in addition to the *cis-trans* isomerization, we observed a number of trajectories undergoing isomerization into isodiimide ($NNH_2$), which is known to exist in matrix environments.[136] At the end of the simulation time half of the *trans*-diimide molecules have isomerised into the *cis* form, with the process starting already in the initial phase of the NA-MD as in line with the reported isomerization time of ∼25 fs.[82] While most of the trajectories continue with the redistribution of vibrational energy among their six internal degrees of freedom once in the ground electronic state, few of them exhibit a repopulation of the first excited state. In other words, few trajectories in the ground electronic state exhibit a NA hop back to the excited state. While the NRD process then continues again from the excited state, the 6% of population that remains in the excited state at the end of the simulation is mainly due to these population oscillations between the two electronic states. Of those that remained in the $n\pi^*$ state, only two trajectories exhibited oscillations around the first excited state minimum structure without showing any inclination towards deactivation into the ground electronic state. This is in agreement with Handt et al.[82]

Similar observations were made for the *cis* conformer and with the used simulation conditions we have not found any significant differences in NA-MD between the two diimide conformers in gas phase. The observed NRD pathways for diimide conformers are similar to the reported NRD mechanisms of methylated diimide ($H_3C$–N=N–$CH_3$) conformers. The dominating deactivation pathway of the $n\pi^*$ electronic state is the NA population transfer through the CI with the distorted CNNC geometry (torsional angles close to 90°[95]). Reported lifetime for the *trans* methylated conformer is in the range of 90-200 fs,[91,95,96] while the *cis* shows a biexponential decay with lifetimes of 66 and 186 fs.[95]

## 4.3 NA-MD of Diimide in the Condensed Phase

The *trans*-diimide molecule was solvated with 62 water molecules in a periodic cubic box with side length of 11.913 Å. As geometrical parameters obtained from the ground state DFT-based MD at ambient conditions indicate in table 1, water molecules induce only a small perturbation on the system when compared to its vacuum equilibrium counter values.

Table 1: Main geometric parameters of the *trans*- and *cis*-diimide conformers in the condensed and gas phases of the sampled initial conditions for the corresponding NA-MD simulations in comparison to optimized minimum geometry. Values for the ab initio MD in explicit solvent and the vacuum minimum geometry were obtained with the PBE functional. The gas phase was sampled with the Wigner distribution directly at the same level of theory used in subsequent NA-MD simulations (PBE0). The same TZVP-GTH basis set was employed for all calculations. Values for the *cis* conformer are shown in parenthesis.

| | solvated MD | vacuum minimum | gas phase Wigner |
|---|---|---|---|
| $d$(N–N) [Å] | $1.250 \pm 0.020$ | 1.248 | $1.229 \pm 0.036$ |
| | $(1.247 \pm 0.011)$ | (1.243) | $(1.228 \pm 0.032)$ |
| $d$(N–H) [Å] | $1.051 \pm 0.027$ | 1.046 | $1.037 \pm 0.069$ |
| | $(1.057 \pm 0.038)$ | (1.054) | $(1.052 \pm 0.064)$ |
| $\sphericalangle$(H–N–N) [°] | $108.6 \pm 3.4$ | 106.2 | $106.2 \pm 6.1$ |
| | $(112.6 \pm 4.5)$ | (113.2) | $(114.1 \pm 6.2)$ |

The *trans*-diimide six internal vibrational frequencies are perturbed by about $-20$ to $+60$ cm$^{-1}$ when compared to corresponding vacuum frequencies (for details see the Supporting Information). Formation of weak hydrogen bonds between the diimide and water molecules is observed during the ground state NVT ab initio MD trajectory. This is clearly indicated in figure 7a with the peaks at 1.85 Å and 2.05 Å of the $N_{dii.}H_{wat.}$ and $H_{dii.}O_{wat.}$ radial distribution functions, respectively. Their intensities, which are roughly half their corresponding maximum values, comply with the observation that the diimide-water hydrogen bonds are present only half of the propagation time. It is more probable to observe one NH group interacting with the oxygen atom of the nearby water molecule and the other NH group loose, than seeing both interacting at the same time. However, while one NH group interacts with the oxygen atom, the other group forms the O–H$\cdots$N hydrogen bond with a neighboring water molecule. Such a configuration is captured in figure 7b. The two types of

hydrogen bonds then alternate between the two NH groups during the dynamics. The first peak of the $N_{dii.}O_{wat.}$ distribution function reveals that the average N$\cdots$O hydrogen bond length is 2.85 Å, which is almost identical to the measured OO distance of pure water.[137] The presence of the maxima in the range of $3-4$ Å for all displayed distribution functions indicates the size of the first water solvation shell structured around the diimide, which consists of about 14-18 water molecules.

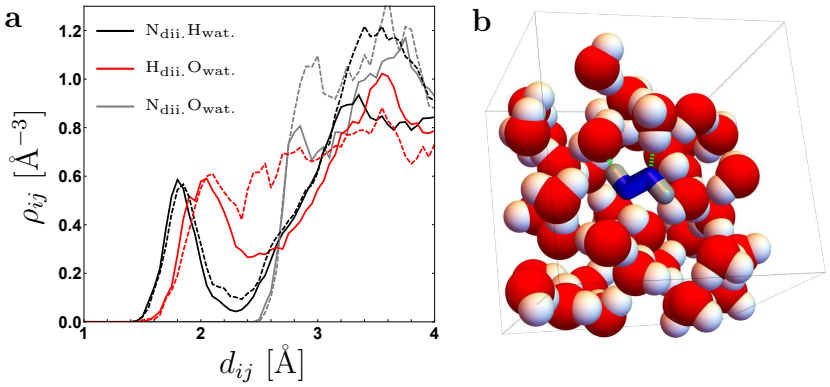


Figure 7: a) Radial distribution functions for the *trans*- and *cis*-diimide solvated in water. The full black, red, and gray lines represent diimide nitrogen–water hydrogen ($N_{dii.}H_{wat.}$), diimide hydrogen–water oxygen ($H_{dii.}O_{wat.}$), and diimide nitrogen–water oxygen ($N_{dii.}O_{wat.}$) radial distribution functions, respectively. The *cis* conformer values are shown with dashed lines. b) Illustration of the *trans*-diimide in a periodic water box with water molecules removed from the front part of the box. The green dashed lines indicate hydrogen bonds between diimide and water molecules.

As for the first excited state of solvated *trans*-diimide in water, the calculated vertical excitation on an ensemble of 100 randomly selected NVT geometries is $4.45 \pm 0.14$ eV at the PBE0-ΔSCF level. Because the vertical excitation of the aforementioned ensemble sampled in vacuum is $4.46 \pm 0.26$ eV, one can conclude that the solvent has almost no effect on the excited electronic state energies. This absence of any significant solvent induced shift is in line with experimental observation,[86] confirming no significant perturbation of the diimide system by the water molecules. A direct comparison of the $n\pi^*$ excitation energy ($4.45 \pm 0.14$ eV) with the experimentally determined absorption maximum (3.44 eV[86]) suggests that ΔSCF overestimates the first singlet excited state.

For the NA-MD, 50 trajectories were propagated to a total length of 50 fs. The initial phase of dynamics resembles that of the *trans*-diimide in gas phase (see Fig. 8). Nonetheless, in this NA-MD only four trajectories have hopped to the ground electronic state (see the full red line in Fig. 8b), compared to 60% of trajectories within the first 50 fs of the gas phase.

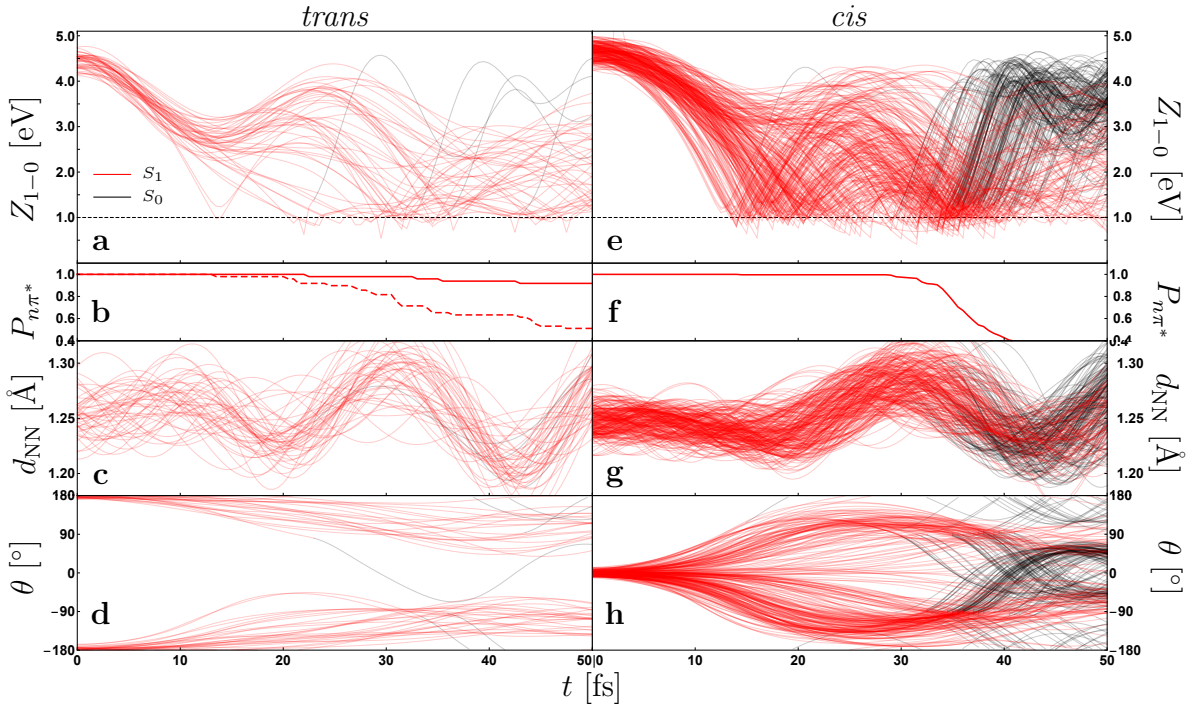


Figure 8: Evolution of 50 and 270 NA-MD trajectories for solvated *trans*-diimide (left) and solvated *cis*-diimide (right), respectively. Only the first 50 fs of the simulation are displayed for the *cis*-diimide. a) and e) Energy difference between the first excited and ground electronic states. b) and f) Average population of the first excited state (full red line). In figure b the red dashed line shows the average population obtained by irreversible forced switching to the ground state which was enforced when the corresponding trajectory energy difference falls below 1 eV. c) and g) N=N bond lengths for the same trajectories. d) and h) The torsional angle $\theta$ between the two NH groups along each trajectory. Lines in figures a, c, d, e, g and h are colored red (black) if the corresponding trajectory is in the first excited (ground) electronic state.

Such a low rate of population transfer to the ground electronic state can be partly traced to the initial conditions. Standard deviations of geometrical parameters for the condensed phase ensemble are smaller than the ones for the gas phase (see table 1). Note that the mean values mainly differ because the gas phase was directly sampled using the PBE0 functional.

This is because the initial conditions for the condensed phase were obtained from an ab initio MD trajectory which generally samples a narrower part of the configuration space than the thermalized Wigner distribution function at the same temperature. The ratio of initial average kinetic energies between the solvated and the isolated diimide is almost three times in favor of the latter. Consequences of such different initial conditions are evident in the first 20 fs of the NA-MD between the solvated and isolated *trans*-diimide, as within this time the fraction of trajectories reaching energy of 1 eV, or lower, is tenfold in the gas phase. We also observed that spikes associated with SCF ground state energy instabilities are more frequent in the gas phase due to the more rapid change of geometry around the distorted structures with $\theta = 90°$. To overcome the small depopulation rate from the dynamics in the condensed system and estimate its excited state lifetime, instead of hops, occurrences when the energy gap decreased below a certain threshold were accounted instead. Within this approach, the population for each trajectory is assumed to have switched completely to the lower state at the first instance the energy gap becomes smaller than 1 eV. We fitted this forced population evolution (designated with the dashed red line in figure 8b) with a monoexponential decay function $\exp(-(t - t_0)/\tau)$, which, by adding the obtained $\tau$ and $t_0$ gives a lifetime of 62 fs. During the dynamics, some hydrogen bonds between the diimide and water molecules were easily broken once the diimide system underwent its torsional distortion around the N=N bond in the excited state, while some remain. Because of the short simulation time relative to the diffusion constant of water, no significant change of the solvation structure was observed. The number of trajectories undergoing NRD mechanism is insufficient to reveal the effect of the water on the *trans*-diimide excited state dynamics.

In order to capture the effects of the environment on the NRD pathways of the *cis* conformer $n\pi^*$ excited state, we simulated its NA-MD in a smaller cubic periodic box with side length of 8.987 Å and 29 water molecules. The size of the box is sufficient to incorporate the first solvation shell. Geometric parameters of the *cis*-diimide system show no significant perturbation by the surrounding water molecules when compared to corresponding

vacuum equilibrium values (see table 1). Influence of water molecules is more exhibited on the perturbation of the ground state's asymmetric and symmetric N–H stretch vibrations while their frequencies are blue-shifted by 185 and 110 $cm^{-1}$, respectively, to corresponding vacuum values. The perturbation of the remaining four normal modes is similar to those of the *trans* conformer (for details see the Supporting Information). Radial distribution functions, when compared to values of the *trans* conformer in Fig. 7, show that the N–H$\cdots$O hydrogen bonding pattern is significantly altered. A more detailed analysis reveals that a water molecule can exchange between the two NH groups, i.e., a water molecule initially bound to one NH group can move to the other NH group due to the *cis* orientation of the two N–H bonds. In average, as seen in the distribution of oxygen atoms around each NH group (see the Supporting Information), the water molecule has a high probability of being between the two NH groups, so the N–H$\cdots$O hydrogen bond is less colinear compared to the solvated *trans*-diimide. This is favorable as a polar water molecule moves in the proximity of the permanent electric dipole moment of the *cis* system (vacuum value is 3 D at the PBE/TZVP level). As a consequence, the hydrogen bond is in average weaker in the solvated *cis* conformer.

For *cis*-diimide in the condensed phase NA-MD 270 trajectories were propagated for 500 time steps. Again, the NRD mechanism is identical to the gas phase case, while the initial 50 fs are analog to the *trans* conformer in the condensed phase (see Fig. 8). Full trajectories are given in the Supporting Information. Statistics reveals that the first excited state also decays with a biexponential rate (see Fig. 9). Its shorter lifetime component is almost identical to the gas phase value, while the slower lifetime component is 50% larger. Apart from the lower initial kinetic energy of the diimide in the condensed phase, we now identify other contributing factors that prolong the excited state lifetime. On one hand, there is the thermostatic effect of the water molecules on the photoexcited diimide. The kinetic energy gained in the excited electronic state from the relaxation of diimide from its Franck-Condon region to the local excited state minimum is drained away by the surrounding

water molecules. This can be clearly seen in the evolution of the mean kinetic energy for trajectories that remain in the excited electronic state by the end of the simulation. As figure 9b shows, the initial oscillation of this mean kinetic energy attenuates and the system settles in the minimum of the excited electronic state. All trajectories within this set ended in the excited state minimum. As the kinetic energy reduces, the coupling between electronic states also reduces, which consequentially prolongs the deactivation time. In the case of the LZ algorithm (8) this is directly influenced by reducing $\ddot{Z}_{ij}$, or in Tully's FS-SH by reducing the $\langle\psi_i|\, d/dt\, |\psi_j\rangle$, as energies and wave functions change slower with time, respectively, when the nuclear velocities reduce.

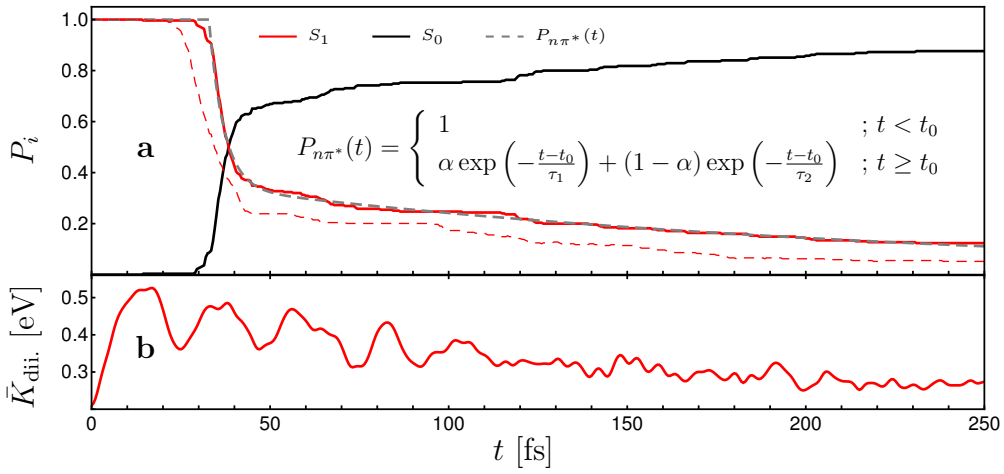


Figure 9: a) Evolution of the excited (red line) and ground (black) electronic state populations of the ensemble of solvated *cis*-diimide. The gray dashed line shows the fitted biexponential decay function (in inset) of the excited state. The two lifetimes are $t_0 + \tau_1 = 37$ fs and $t_0 + \tau_2 = 226$ fs. The population of the *cis* excited state conformer in gas phase is given for comparison (red dashed line). Its two corresponding lifetimes are 32 fs and 148 fs. Other fitted values are given in the Supporting Information. b) Evolution of the mean diimide subsystem kinetic energy ($\bar{K}_{\text{dii.}}$) within the periodic box sampled from trajectories which remain in the excited electronic state for the whole simulation time.

Figures 10a and c show that the hydrogen bonding pattern between the diimide and neighboring water molecules is preserved for the aforementioned set of trajectories remaining in the excited state. As the N–H bonds distort into opposite directions during the dynamics the $\text{H}_{\text{dii.}} \cdots \text{O}_{\text{wat.}}$ radial distribution function also evolves into the shape corresponding more

to the *trans* conformer (compare to Fig. 7). In case of trajectories deactivating to the ground electronic state, once the absorbed energy is converted into the kinetic energy upon a NA hop, the sudden increase of diimide velocities and nearby water molecules is enough to disrupt the hydrogen bond interactions as clearly seen by the reduction of the first peaks in figures 10b and d. The solvation shell, however, remains intact while the $N_{dii.}O_{wat.}$ radial distribution functions do not change in time nor display dependence on the electronic states. This is in line with the observation by Cattaneo and Persico on the cooling of the vibrationally excited methylated diimide during and after the NRD.[91] As expected, no repopulation of excited electronic state was observed due to a significantly larger number of degrees of freedom among which the absorbed photon energy gets distributed. An analogue cooling of vibrationally excited diimide in ground electronic state is observed. No isodiimide formation occurs for the solvated system during the simulation time, while the *cis* to *trans* ratio at the end is 2 : 1.

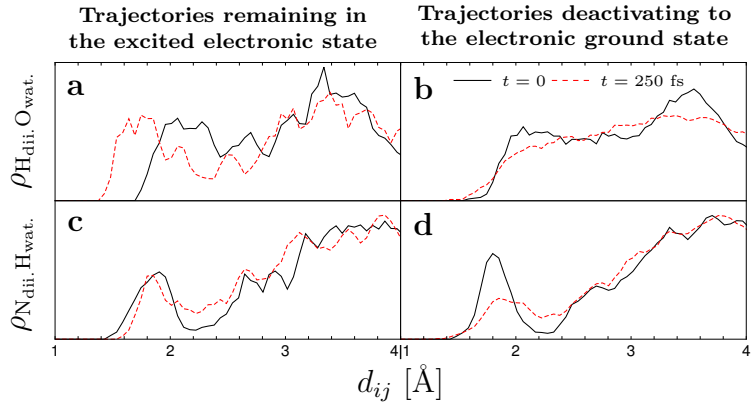


Figure 10: Radial distribution functions for the solvated *cis*-diimide computed at the first (black line) and last (dashed red line) step of NA-MD simulations. Images a and b show the $H_{dii.}O_{wat.}$, while c and d display the $N_{dii.}H_{wat.}$ radial distribution functions. Distance between atom pairs ($d_{ij}$) designates distance for $H_{dii.}O_{wat.}$ in images a and b, and for $N_{dii.}H_{wat.}$ in images c and d. Within images a and c the system remains in the first excited electronic state, while in images b and d it relaxes to the ground state.

The statistics for the solvated *trans*-diimide is insufficient to observe the cooling effect and changes in the hydrogen bonding pattern (see an analogue of Fig. S6 in the Supporting Information). Nonetheless, the differences in the ground state N–H$\cdots$O hydrogen bonds

between the *trans* and *cis* conformers might explain why the deactivation rate in the first conformer is not as rapid as in the latter, i.e., why are there no fast-deactivating trajectories observed in *trans*-diimide NA-MD. The distribution of oxygen atoms around the NH groups has shown that the N–H$\cdots$O hydrogen bond is in average weaker in the *cis* than in the *trans* conformer, making the torsion of the N=N bond less influenced by the neighbouring water molecules in the *cis* conformer. In *trans*-diimide the more stable hydrogen bond might be slowing the torsional motion in the initial phase of NA-MD. This is in line with the observation that the same hydrogen bonds are preserved in the vibrationally cooled *cis* conformer trajectories that remained in the first electronic excited state (see Fig. 10a and c).

# 5 Conclusions

In this work we have presented an approach for NA-MD in the condensed phase using the CP2K program package. This was achieved by utilizing the Gaussian and plane waves approach with periodic boundary conditions. For the systems studied in this work, a $\Delta$SCF procedure based on restricted KS orbitals for efficient calculation of singlet excited electronic state energies and corresponding gradients was carried out. During the SCF optimization of the excited state electronic densities the corresponding KS orbital occupation numbers were fixed and rounded to 0, 1, or 2. The latter criterion has been relaxed whenever the SCF would exhibit convergence issues and a TD-DFT calculation was employed to update the occupation numbers. Although Tully's FS-SH can in principle be used with our implementation, Landau-Zener formulation of SH was used to determine the hopping probabilities among electronic states, avoiding the computation of the nonadiabatic coupling terms between electronic states and propagation of the electronic populations as well as decoherence corrections. We have also shown how the calculation of nonadiabatic coupling elements between ground and excited electronic state can be simplified, but also raised doubt in the general validity

of using KS orbitals for the construction of nonadiabatic coupling terms within the ΔSCF formulation. To our best knowledge, this is the first use of the CP2K code to calculate electronic excited states at the ΔSCF level and to conduct Landau-Zener TSH-NA-MD simulations on periodic systems.

The implementation successfully reproduced the NRD pathway of the photoexcited singlet $\pi\pi^*$ state of ethylene in gas phase and the corresponding excited state lifetime. The diimide system was studied in the condensed phase using a periodic water box as well as in gas phase for comparison. While comparison between equilibrated structures in the ground electronic state for the two different phases shows no significant perturbation of the diimide system by the surrounding water molecules, excited state NA-MD simulations display that the hydrogen bonds between the solute and the solvent are preserved in the excited state and how they couple the solute to the solvent, where the latter acts as a thermostat, cooling the system significantly in the initial stages of excited state evolution. Aside from the difference in the initial conditions for the gas and condensed phase NA-MDs, we account these effects partly responsible for the observed prolongation of the diimide's excited state lifetime in the condensed phase. No significant differences between the two conformers could be observed in the gas phase, and their NA-MD are virtually identical, yielding equal deactivation kinetics. However, a more frequent exchange of the water molecule between the two NH groups as well as the presence of the permanent electric dipole moment in the *cis*-diimide weakens the hydrogen bond between the solute and the solvent. This makes the torsional motion easier in the initial phase of NA-MD due to which the solvated *cis* conformer kinetics resembles more the one in gas phase. On the other hand the stronger hydrogen bond in *trans*-diimide might be responsible for the absence of the fast-decaying component. In the excited state, the two conformers become indistinguishable while they evolve around their common excited state minimum structure. Thus distinctions in their NRD kinetics arise from the subtle difference the two conformers impose on the solvent molecules around them in their ground electronic state. Findings on the diimide systems are consistent with previous observations made on

the methylated diimide ($H_3C$–N=N–$CH_3$).

In summary, we have shown how the CP2K's all-atom DFT simulation capabilities can be further efficiently expanded from ground to excited electronic states and used for trajectory surface hopping, introducing another potential toolset for NA-MD of condensed phase systems. Since this approach can be used with periodic boundary conditions, detailed studies of photovoltaic materials, photoactive molecules adsorbed on surfaces as well as environmental effects for liquids, such as the one studied in this work, may be of future interest.

## Acknowledgement

The work has been supported by the University of Zurich and the Swiss National Science Foundation (grant no. PP00P2 170667). We thank the Swiss National Supercomputing Center for computing resources (project IDs: s875 and s788).

## Supporting Information Available

Formulation of the Tully's fewest-switch surface hopping procedure in the restricted KS orbital ΔSCF; Investigation of nonadiabatic couplings; Sampling of the NA-MD initial conditions; Details of the diimide's CASSCF calculations; Vibrational analysis of solvated diimide systems; Distribution of water molecules in the solvated diimide systems; Lifetime of energy-shifted *trans*-diimide $n\pi^*$ excited electronic state; Full NA-MD trajectories of the solvated *cis*-diimide.

## References

(1) Eckert-Maksić, M.; Vazdar, M.; Ruckenbauer, M.; Barbatti, M.; Müller, T.; Lischka, H. Matrix-controlled photofragmentation of formamide: Dynamics simulation in argon by nonadiabatic QM/MM method. *Phys. Chem. Chem. Phys.* **2010**, *12*, 12719–12726.

(2) Tavernelli, I.; Curchod, B. F.; Rothlisberger, U. Nonadiabatic molecular dynamics with solvent effects: A LR-TDDFT QM/MM study of ruthenium (II) tris (bipyridine) in water. *Chem. Phys.* **2011**, *391*, 101–109.

(3) Virshup, A. M.; Levine, B. G.; Martínez, T. J. Steric and electrostatic effects on photoisomerization dynamics using QM/MM ab initio multiple spawning. *Theor. Chem. Acc.* **2014**, *133*, 1506.

(4) Hoche, J.; Schmitt, H. C.; Humeniuk, A.; Fischer, I.; Mitrić, R.; Röhr, M. I. The mechanism of excimer formation: An experimental and theoretical study on the pyrene dimer. *Phys. Chem. Chem. Phys.* **2017**, *19*, 25002–25015.

(5) Mališ, M.; Novak, J.; Zgrablić, G.; Parmigiani, F.; Došlić, N. Mechanism of ultrafast non-reactive deactivation of the retinal chromophore in non-polar solvents. *Phys. Chem. Chem. Phys.* **2017**, *19*, 25970–25978.

(6) Levi, G.; Pápai, M.; Henriksen, N. E.; Dohn, A. O.; Møller, K. B. Solution Structure and Ultrafast Vibrational Relaxation of the PtPOP Complex Revealed by ΔSCF-QM/MM Direct Dynamics Simulations. *J. Phys. Chem. C* **2018**, *122*, 7100–7119.

(7) Nogueira, J. J.; Roßbach, S.; Ochsenfeld, C.; González, L. Effect of DNA Environment on Electronically Excited States of Methylene Blue Evaluated by a Three-Layered QM/QM/MM ONIOM Scheme. *J. Chem. Theory Comput.* **2018**, *14*, 4298–4308.

(8) Fang, Y.-G.; Peng, L.-Y.; Liu, X.-Y.; Fang, W.-H.; Cui, G. QM/MM nonadiabatic dynamics simulation on ultrafast excited-state relaxation in osmium(II) compounds in solution. *Comput. Theor. Chem.* **2019**, *1155*, 90–100.

(9) Giannini, S.; Carof, A.; Ellis, M.; Yang, H.; Ziogos, O. G.; Ghosh, S.; Blumberger, J. Quantum localization and delocalization of charge carriers in organic semiconducting crystals. *Nat. Commun.* **2019**, *10*, 1–12.

(10) Lin, Y.-l.; Gao, J. Solvatochromic Shifts of the $n \rightarrow \pi^*$ Transition of Acetone from Steam Vapor to Ambient Aqueous Solution: A Combined Configuration Interaction QM/MM Simulation Study Incorporating Solvent Polarization. *J. Chem. Theory Comput.* **2007**, *3*, 1484–1493.

(11) Sneskov, K.; Schwabe, T.; Christiansen, O.; Kongsted, J. Scrutinizing the effects of polarization in QM/MM excited state calculations. *Phys. Chem. Chem. Phys.* **2011**, *13*, 18551.

(12) Sifain, A. E.; Bjorgaard, J. A.; Nelson, T. R.; Nebgen, B. T.; White, A. J.; Gifford, B. J.; Gao, D. W.; Prezhdo, O. V.; Fernandez-Alberti, S.; Roitberg, A. E.; Tretiak, S. Photoexcited Nonadiabatic Dynamics of Solvated Push–Pull $\pi$-Conjugated Oligomers with the NEXMD Software. *J. Chem. Theory Comput.* **2018**, *14*, 3955–3966.

(13) Liang, W.; Chapman, C. T.; Ding, F.; Li, X. Modeling Ultrafast Solvated Electronic Dynamics Using Time-Dependent Density Functional Theory and Polarizable Continuum Model. *J. Phys. Chem. A* **2012**, *116*, 1884–1890.

(14) Ghosh, S.; Asher, J. C.; Gagliardi, L.; Cramer, C. J.; Govind, N. A semiempirical effective Hamiltonian based approach for analyzing excited state wave functions and computing excited state absorption spectra using real-time dynamics. *J. Chem. Phys.* **2019**, *150*, 104103.

(15) Pal, S.; Trivedi, D. J.; Akimov, A. V.; Aradi, B.; Frauenheim, T.; Prezhdo, O. V. Nonadiabatic Molecular Dynamics for Thousand Atom Systems: A Tight-Binding Approach toward PYXAID. *J. Chem. Theory Comput.* **2016**, *12*, 1436–1448.

(16) Stojanović, L.; Aziz, S. G.; Hilal, R. H.; Plasser, F.; Niehaus, T. A.; Barbatti, M. Nonadiabatic Dynamics of Cycloparaphenylenes with TD-DFTB Surface Hopping. *J. Chem. Theory Comput.* **2017**, *13*, 5846–5860.

(17) Titov, E.; Humeniuk, A.; Mitrić, R. Exciton localization in excited-state dynamics of a tetracene trimer: a surface hopping LC-TDDFTB study. *Phys. Chem. Chem. Phys.* **2018**, *20*, 25995–26007.

(18) Spencer, J.; Gajdos, F.; Blumberger, J. FOB-SH: Fragment orbital-based surface hopping for charge carrier transport in organic and biological molecules and materials. *J. Chem. Phys.* **2016**, *145*, 064102.

(19) Akimov, A. V. Nonadiabatic Molecular Dynamics with Tight-Binding Fragment Molecular Orbitals. *J. Chem. Theory Comput.* **2016**, *12*, 5719–5736.

(20) Franco de Carvalho, F.; Tavernelli, I. Nonadiabatic dynamics with intersystem crossings: A time-dependent density functional theory implementation. *J. Chem. Phys.* **2015**, *143*, 224105.

(21) Capano, G.; Penfold, T. J.; Chergui, M.; Tavernelli, I. Photophysics of a copper phenanthroline elucidated by trajectory and wavepacket-based quantum dynamics: A synergetic approach. *Physical Chemistry Chemical Physics* **2017**, *19*, 19590–19600.

(22) Wang, X.; Long, R. Oxidation Notably Accelerates Nonradiative Electron–Hole Recombination in $MoS_2$ by Different Mechanisms: Time-Domain Ab Initio Analysis. *J. Phys. Chem. Lett.* **2020**, 4086–4092.

(23) Casida, M. E. Time-dependent density-functional theory for molecules and molecular solids. *Comp. Theor. Chem.* **2009**, *914*, 3–18.

(24) Ullrich, C. A. *Time-Dependent Density-Functional Theory: Concepts and Applications*; Oxford University Press Inc.: New York, 2012.

(25) Ziegler, T.; Rauk, A.; Baerends, E. J. On the calculation of multiplet energies by the hartree-fock-slater method. *Theor. Chim. Acta* **1977**, *43*, 261–271.

(26) Jones, R. O.; Gunnarsson, O. The density functional formalism, its applications and prospects. *Rev. Mod. Phys.* **1989**, *61*, 689–746.

(27) Hellman, A.; Razaznejad, B.; Lundqvist, B. Potential-energy surfaces for excited states in extended systems. *J. Chem. Phys.* **2004**, *120*, 4593–4602.

(28) Gavnholt, J.; Olsen, T.; Engelund, M.; Schiøtz, J. $\Delta$ self-consistent field method to obtain potential energy surfaces of excited molecules on surfaces. *Phys. Rev. B* **2008**, *78*, 075441.

(29) Maurer, R. J.; Reuter, K. Excited-state potential-energy surfaces of metal-adsorbed organic molecules from linear expansion $\Delta$-self-consistent field density-functional theory ($\Delta$SCF-DFT). *J. Chem. Phys.* **2013**, *139*, 014708.

(30) Behler, J.; Reuter, K.; Scheffler, M. Nonadiabatic effects in the dissociation of oxygen molecules at the Al(111) surface. *Phys. Rev. B Condens. Matter* **2008**, *77*, 115421.

(31) Maurer, R. J.; Reuter, K. Assessing computationally efficient isomerization dynamics: $\Delta$SCF density-functional theory study of azobenzene molecular switching. *J. Chem. Phys.* **2011**, *135*, 224303.

(32) Mackrodt, W. C.; Salustro, S.; Civalleri, B.; Dovesi, R. Low energy excitations in NiO based on a direct $\Delta$-SCF approach. *J. Condens. Matter Phys.* **2018**, *30*, 495901.

(33) Kowalczyk, T.; Yost, S. R.; Voorhis, T. V. Assessment of the $\Delta$SCF density functional theory approach for electronic excitations in organic dyes. *J. Chem. Phys.* **2011**, *134*, 054128.

(34) Baruah, T.; Olguin, M.; Zope, R. R. Charge transfer excited state energies by perturbative delta self consistent field method. *J. Chem. Phys.* **2012**, *137*, 084316.

(35) Pradhan, E.; Sato, K.; Akimov, A. V. Non-adiabatic molecular dynamics with $\Delta$SCF excited states. *J. Condens. Matter Phys.* **2018**, *30*, 484002.

(36) Moore, B.; Sun, H.; Govind, N.; Kowalski, K.; Autschbach, J. Charge-Transfer Versus Charge-Transfer-Like Excitations Revisited. *J. Chem. Theory Comput.* **2015**, *11*, 3305–3320.

(37) Crespo-Otero, R.; Barbatti, M. Recent Advances and Perspectives on Nonadiabatic Mixed Quantum–Classical Dynamics. *Chem. Rev.* **2018**, *118*, 7026–7068.

(38) Smith, B.; Akimov, A. V. Modeling nonadiabatic dynamics in condensed matter materials: some recent advances and applications. *J. Condens. Matter Phys.* **2020**, *32*, 073001.

(39) Nelson, T. R.; White, A. J.; Bjorgaard, J. A.; Sifain, A. E.; Zhang, Y.; Nebgen, B.; Fernandez-Alberti, S.; Mozyrsky, D.; Roitberg, A. E.; Tretiak, S. Non-adiabatic Excited-State Molecular Dynamics: Theory and Applications for Modeling Photophysics in Extended Molecular Materials. *Chem. Rev.* **2020**, acs.chemrev.9b00447.

(40) Curchod, B. F. E.; Rothlisberger, U.; Tavernelli, I. Trajectory-Based Nonadiabatic Dynamics with Time-Dependent Density Functional Theory. *ChemPhysChem* **2013**, *14*, 1314–1340.

(41) Wang, L.; Akimov, A.; Prezhdo, O. V. Recent Progress in Surface Hopping: 2011–2015. *J. Phys. Chem. Lett.* **2016**, *7*, 2100–2112.

(42) Curchod, B. F. E.; Martínez, T. J. Ab Initio Nonadiabatic Quantum Molecular Dynamics. *Chem. Rev.* **2018**, *118*, 3305–3336.

(43) Agostini, F.; Curchod, B. F. E. Different flavors of nonadiabatic molecular dynamics. *Wiley Interdiscip. Rev. Comput. Mol. Sci.* **2019**, *9*, e1417.

(44) Nakamura, H. *Introduction to Nonadiabatic Dynamics*; Worl Scientific, 2019.

(45) Tully, J. C. Molecular dynamics with electronic transitions. *J. Chem. Phys.* **1990**, *93*, 1061–1071.

(46) Landau, L. D. On the theory of transfer of energy at collisions II. *Phys. Z. Sowjetunion* **1932**, *2*, 46.

(47) Zener, C. Non-Adiabatic Crossing of Energy Levels. *Proc. R. Soc. A* **1932**, *137*, 696–702.

(48) Zhu, C.; Teranishi, Y.; Nakamura, H. *Adv. Chem. Phys.*; John Wiley & Sons, Ltd, 2007; pp 127–233.

(49) Belyaev, A. K.; Lebedev, O. V. Nonadiabatic nuclear dynamics of atomic collisions based on branching classical trajectories. *Phys. Rev. A* **2011**, *84*, 014701.

(50) Xie, W.; Domcke, W. Accuracy of trajectory surface-hopping methods: Test for a two-dimensional model of the photodissociation of phenol. *J. Chem. Phys.* **2017**, *147*.

(51) Xie, W.; Sapunar, M.; Došlić, N.; Sala, M.; Domcke, W. Assessing the performance of trajectory surface hopping methods: Ultrafast internal conversion in pyrazine. *J. Chem. Phys.* **2019**, *150*, 154119.

(52) Subotnik, J. E.; Jain, A.; Landry, B.; Petit, A.; Ouyang, W.; Bellonzi, N. Understanding the Surface Hopping View of Electronic Transitions and Decoherence. *Annu. Rev. Phys. Chem.* **2016**, *67*, 387–417.

(53) Lin, M.-F.; Kochat, V.; Krishnamoorthy, A.; Bassman, L.; Weninger, C.; Zheng, Q.; Zhang, X.; Apte, A.; Tiwary, C. S.; Shen, X.; Li, R.; Kalia, R.; Ajayan, P.; Nakano, A.; Vashishta, P.; Shimojo, F.; Wang, X.; Fritz, D. M.; Bergmann, U. Ultrafast non-radiative dynamics of atomically thin MoSe2. *Nat. Commun.* **2017**, *8*, 1745.

(54) Bassman, L.; Krishnamoorthy, A.; Kumazoe, H.; Misawa, M.; Shimojo, F.; Kalia, R. K.; Nakano, A.; Vashishta, P. Electronic Origin of Optically-Induced Sub-Picosecond Lattice Dynamics in $MoSe_2$ Monolayer. *Nano Lett.* **2018**, *18*, 4653–4658.

(55) Hafner, J.; Kresse, G. *Properties of Complex Inorganic Solids*; Springer US: Boston, MA, 1997; pp 69–82.

(56) Shimojo, F.; Fukushima, S.; Kumazoe, H.; Misawa, M.; Ohmura, S.; Rajak, P.; Shimamura, K.; Bassman, L.; Tiwari, S.; Kalia, R. K.; Nakano, A.; Vashishta, P. QXMD: An open-source program for nonadiabatic quantum molecular dynamics. *SoftwareX* **2019**, *10*, 100307.

(57) Giannozzi, P.; Baroni, S.; Bonini, N.; Calandra, M.; Car, R.; Cavazzoni, C.; Ceresoli, D.; Chiarotti, G. L.; Cococcioni, M.; Dabo, I.; Dal Corso, A.; de Gironcoli, S.; Fabris, S.; Fratesi, G.; Gebauer, R.; Gerstmann, U.; Gougoussis, C.; Kokalj, A.; Lazzeri, M.; Martin-Samos, L.; Marzari, N.; Mauri, F.; Mazzarello, R.; Paolini, S.; Pasquarello, A.; Paulatto, L.; Sbraccia, C.; Scandolo, S.; Sclauzero, G.; Seitsonen, A. P.; Smogunov, A.; Umari, P.; Wentzcovitch, R. M. QUANTUM ESPRESSO: a modular and open-source software project for quantum simulations of materials. *J. Condens. Matter Phys.* **2009**, *21*, 395502.

(58) Akimov, A. V. Libra: An open-Source "methodology discovery" library for quantum and classical dynamics simulations. *J. Comput. Chem.* **2016**, *37*, 1626–1649.

(59) CP2K Program Package, CP2K Developers Group, Version 6.1, https://www.cp2k.org/.

(60) Hutter, J.; Iannuzzi, M.; Schiffmann, F.; VandeVondele, J. cp2k: atomistic simulations of condensed matter systems. *WIRES Comput. Mol. Sci.* **2014**, *4*, 15–25.

(61) Sedova, A.; Eblen, J. D.; Budiardja, R.; Tharrington, A.; Smith, J. C. High-Performance Molecular Dynamics Simulation for Biological and Materials Sciences: Challenges of Performance Portability. 2018 IEEE/ACM International Workshop on Performance, Portability and Productivity in HPC (P3HPC). 2018; pp 1–13.

(62) Iannuzzi, M.; Chassaing, T.; Wallman, T.; Hutter, J. Ground and Excited State Density Functional Calculations with the Gaussian and Augmented-Plane-Wave Method. *CHIMIA* **2005**, *59*, 499–503.

(63) Ben-Nun, M.; Martínez, T. J. Ab initio molecular dynamics study of cis–trans photoisomerization in ethylene. *Chem. Phys. Lett.* **1998**, *298*, 57–65.

(64) Ben-Nun, M.; Martıínez, T. J. Photodynamics of ethylene: ab initio studies of conical intersections. *Chem. Phys.* **2000**, *259*, 237–248.

(65) Viel, A.; Krawczyk, R. P.; Manthe, U.; Domcke, W. Photoinduced dynamics of ethene in the N, V, and Z valence states: A six-dimensional nonadiabatic quantum dynamics investigation. *J. Chem. Phys.* **2004**, *120*, 11000–11010.

(66) Barbatti, M.; Paier, J.; Lischka, H. Photochemistry of ethylene: A multireference configuration interaction investigation of the excited-state energy surfaces. *J. Chem. Phys.* **2004**, *121*, 11614–11624.

(67) Barbatti, M.; Ruckenbauer, M.; Lischka, H. The photodynamics of ethylene: A surface-hopping study on structural aspects. *J. Chem. Phys.* **2005**, *122*, 174307.

(68) Barbatti, M.; Granucci, G.; Persico, M.; Lischka, H. Semiempirical molecular dynamics investigation of the excited state lifetime of ethylene. *Chem. Phys. Lett.* **2005**, *401*, 276–281.

(69) Tao, H.; Allison, T. K.; Wright, T. W.; Stooke, A. M.; Khurmi, C.; Van Tilborg, J.; Liu, Y.; Falcone, R. W.; Belkacem, A.; Martinez, T. J. Ultrafast internal conversion in ethylene. I. the excited state lifetime. *J. Chem. Phys.* **2011**, *134*.

(70) Mori, T.; Glover, W. J.; Schuurman, M. S.; Martinez, T. J. Role of Rydberg states in the photochemical dynamics of ethylene. *J. Phys. Chem. A* **2012**, *116*, 2808–2818.

(71) Sellner, B.; Barbatti, M.; Müller, T.; Domcke, W.; Lischka, H. Ultrafast non-adiabatic dynamics of ethylene including Rydberg states. *Mol. Phys.* **2013**, *111*, 2439–2450.

(72) Champenois, E. G.; Shivaram, N. H.; Wright, T. W.; Yang, C. S.; Belkacem, A.; Cryan, J. P. Involvement of a low-lying Rydberg state in the ultrafast relaxation dynamics of ethylene. *J. Chem. Phys.* **2016**, *144*.

(73) Baird, N. C.; Swenson, J. R. Quantum Organic Photochemistry. IV. The Photoisomerization of Diimide and Azoalkanes. *Can. J. Chem.* **1973**, *51*, 3097–3101.

(74) Vasudevan, K.; Peyerimhoff, S. D.; Buenker, R. J.; Kammer, W. E.; Hsu, H.-l. Theoretical study of the electronic spectrum of diimide by ab initio methods. *Chem. Phys.* **1975**, *7*, 187–209.

(75) Spears, L. G.; Hutchinson, J. S. Classical dynamics of *trans*-diimide: Intramolecular vibrational relaxation involving an active torsion. *J. Chem. Phys.* **1988**, *88*, 240–249.

(76) Del Bene, J. E.; Kim, K.; Shavitt, I. An *ab initio* study of symmetry breaking in calculations on the first excited singlet state of $N_2H_2$. *Can. J. Chem.* **1991**, *69*, 246–250.

(77) Kim, K.; Shavitt, I.; Del Bene, J. E. Theoretical study of the di-imide ($N_2H_2$) molecule in ground and $n \rightarrow \pi^*$ excited states. *J. Chem. Phys.* **1992**, *96*, 7573–7579.

(78) Angeli, C.; Cimiraglia, R.; Hofmann, H.-J. On the competition between the inversion and rotation mechanisms in the cis-trans thermal isomerization of diazene. *Chem. Phys. Lett.* **1996**, *259*, 276–282.

(79) Sokalski, W. A.; Góra, R. W.; Bartkowiak, W.; Kobyliński, P.; Sworakowski, J.; Chyla, A.; Leszczyński, J. New theoretical insight into the thermal *cis–trans* isomerization of azo compounds: Protonation lowers the activation barrier. *J. Chem. Phys.* **2001**, *114*, 5504–5508.

(80) Sindhu, A.; Pradhan, R.; Lourderaj, U.; Paranjothy, M. Theoretical investigation of the isomerization pathways of diazenes: torsion *vs.* inversion. *Phys. Chem. Chem. Phys.* **2019**, *21*, 15678–15685.

(81) Tavernelli, I.; Röhrig, U. F.; Rothlisberger, U. Molecular dynamics in electronically excited states using time-dependent density functional theory. *Mol. Phys.* **2005**, *103*, 963–981.

(82) Handt, J.; Kunert, T.; Schmidt, R. Fragmentation and cis–trans isomerization of diimide in fs laser-pulses. *Chem. Phys. Lett.* **2006**, *428*, 220–226.

(83) Willis, C.; Back, R. A. Di-imide: Some Physical and Chemical Properties, and the Kinetics and Stoichiometry of the Gas-phase Decomposition. *Can. J. Chem.* **1973**, *51*, 3605–3619.

(84) Willis, C.; Back, R.; Parsons, J. The photochemical decomposition of diimide in the gas phase. *Journal of Photochemistry* **1976**, *6*, 253–264.

(85) Biehl, H.; Stuhl, F. Vacuum-ultraviolet photolysis of $N_2H_2$: Generation of NH fragments. *J. Chem. Phys.* **1994**, *100*, 141–145.

(86) Tang, H. R.; Stanbury, D. M. Direct Detection of Aqueous Diazene: Its UV Spectrum and Concerted Dismutation. *Inorg. Chem.* **1994**, *33*, 1388–1391.

(87) North, S. W.; Longfellow, C. A.; Lee, Y. T. The near ultraviolet photodissociation dynamics of azomethane. *J. Chem. Phys.* **1993**, *99*, 4423–4429.

(88) Cattaneo, P.; Persico, M. Semiclassical treatment of the photofragmentation of azomethane. *Chem. Phys. Lett.* **1998**, *289*, 160–166.

(89) Cattaneo, P.; Granucci, G.; Persico, M. Simulations of condensed phase photochemistry: Cage effect and internal conversion in azoalkanes and nitrosamines. *J. Phys. Chem. A* **1999**, *103*, 3364–3371.

(90) Diau, E. W.; Abou-Zied, O. K.; Scala, A. A.; Zewail, A. H. Femtosecond dynamics of transition states and the concept of concertedness: Nitrogen extrusion of azomethane reactions. *J. Am. Chem. Soc.* **1998**, *120*, 3245–3246.

(91) Cattaneo, P.; Persico, M. Semiclassical simulations of azomethane photochemistry in the gas phase and in solution. *J. Am. Chem. Soc.* **2001**, *123*, 7638–7645.

(92) Diau, E. W.; Zewail, A. H. Femtochemistry of trans-azomethane: A combined experimental and theoretical study. *ChemPhysChem* **2003**, *4*, 445–456.

(93) Granucci, G.; Persico, M. Excited state dynamics with the direct trajectory surface hopping method: Azobenzene and its derivatives as a case study. *Theor. Chem. Acc.* **2007**, *117*, 1131–1143.

(94) Ruckenbauer, M.; Barbatti, M.; Sellner, B.; Muller, T.; Lischka, H. Azomethane: Nonadiabatic photodynamical simulations in solution. *J. Phys. Chem. A* **2010**, *114*, 12585–12590.

(95) Sellner, B.; Ruckenbauer, M.; Stambolić, I.; Barbatti, M.; Aquino, A. J.; Lischka, H. Photodynamics of azomethane: A nonadiabatic surface-hopping study. *J. Phys. Chem. A* **2010**, *114*, 8778–8785.

(96) Ghosh, J.; Bhaumik, S.; Bhattacharya, A. Comparison of internal conversion dynamics of azo and azoxy energetic moieties through the (S1/S0)CI conical Intersection: An ab initio multiple spawning study. *Chem. Phys.* **2018**, *513*, 221–229.

(97) Chai, J.-D. Density functional theory with fractional orbital occupations. *J. Chem. Phys.* **2012**, *136*, 154104.

(98) Warren, R.; Dunlap, B. Fractional occupation numbers and density functional energy gradients within the linear combination of Gaussian-type orbitals approach. *Chem. Phys. Lett.* **1996**, *262*, 384–392.

(99) Gaudoin, R.; Burke, K. Lack of Hohenberg-Kohn Theorem for Excited States. *Phys. Rev. Lett.* **2004**, *93*, 173001.

(100) Hirata, S.; Head-Gordon, M. Time-dependent density functional theory within the Tamm-Dancoff approximation. *Chem. Phys. Lett.* **1999**, *314*, 291–299.

(101) Frank, I.; Hutter, J.; Marx, D.; Parrinello, M. Molecular dynamics in low-spin excited states. *J. Chem. Phys.* **1998**, *108*, 4060–4069.

(102) Gräfenstein, J.; Kraka, E.; Cremer, D. Density functional theory for open-shell singlet biradicals. *Chem. Phys. Lett.* **1998**, *288*, 593–602.

(103) Gräfenstein, J.; Cremer, D. Can density functional theory describe multi-reference systems? Investigation of carbenes and organic biradicals. *Phys. Chem. Chem. Phys.* **2000**, *2*, 2091–2103.

(104) Odelius, M.; Laikov, D.; Hutter, J. Excited state geometries within time-dependent and restricted open-shell density functional theories. *J. Mol. Struct. THEOCHEM* **2003**, *630*, 163–175.

(105) Marx, D.; Hutter, J. *Ab Initio Molecular Dynamics*; Cambridge University Press: Cambridge, 2009.

(106) Kowalczyk, T.; Tsuchimochi, T.; Chen, P. T.; Top, L.; Van Voorhis, T. Excitation energies and Stokes shifts from a restricted open-shell Kohn-Sham approach. *J. Chem. Phys.* **2013**, *138*, 164101.

(107) Billeter, S. R.; Egli, D. Calculation of nonadiabatic couplings with restricted open-shell Kohn-Sham density-functional theory. *J. Chem. Phys.* **2006**, *125*, 224103.

(108) Alary, F.; Boggio-Pasqua, M.; Heully, J. L.; Marsden, C. J.; Vicendo, P. Theoretical characterization of the lowest triplet excited states of the tris-(1,4,5,8-

tetraazaphenanthrene) ruthenium dication complex. *Inorg. Chem.* **2008**, *47*, 5259–5266.

(109) Zagreb surface hopping code, 2018; available from `https://e-cam.readthedocs.io/en/latest/Quantum-Dynamics-Modules/index.html` .

(110) Mališ, M.; Agostini, F.; Sanz-Sanz, C.; Ehrmaier, J.; MacKernan, D.; Lauvergnat, D.; Bonella, S. D3.4.: Quantum Dynamics E-CAM modules III. **2018**,

(111) Sapunar, M.; Piteša, T.; Davidović, D.; Došlić, N. Highly Efficient Algorithms for CIS Type Excited State Wave Function Overlaps. *Journal of Chemical Theory and Computation* **2019**, *15*, 3461–3469, PMID: 31038947.

(112) Topaler, M. S.; Allison, T. C.; Schwenke, D. W.; Truhlar, D. G. Test of Trajectory Surface Hopping Against Accurate Quantum Dynamics for an Electronically Nonadiabatic Chemical Reaction. *J. Phys. Chem. A* **1998**, *102*, 1666–1673.

(113) Adamo, C.; Barone, V. Toward reliable density functional methods without adjustable parameters: The PBE0 model. *J. Chem. Phys.* **1999**, *110*, 6158–6170.

(114) Guidon, M.; Hutter, J.; VandeVondele, J. Auxiliary Density Matrix Methods for Hartree-Fock Exchange Calculations. *J. Chem. Theory Comput.* **2010**, *6*, 2348–2364.

(115) VandeVondele, J.; Hutter, J. Gaussian basis sets for accurate calculations on molecular systems in gas and condensed phases. *J. Chem. Phys.* **2007**, *127*, 114105.

(116) Goedecker, S.; Teter, M.; Hutter, J. Separable dual-space Gaussian pseudopotentials. *Phys. Rev. B* **1996**, *54*, 1703–1710.

(117) Grimme, S.; Antony, J.; Ehrlich, S.; Krieg, H. A consistent and accurate *ab initio* parametrization of density functional dispersion correction (DFT-D) for the 94 elements H-Pu. *J. Chem. Phys.* **2010**, *132*, 154104.

(118) TURBOMOLE V6.6 2014, a development of University of Karlsruhe and Forschungszentrum Karlsruhe GmbH, 1989-2007, TURBOMOLE GmbH, since 2007; available from `http://www.turbomole.com`.

(119) Schirmer, J. Beyond the random-phase approximation: A new approximation scheme for the polarization propagator. *Phys. Rev. A* **1982**, *26*, 2395–2416.

(120) Trofimov, A. B.; Schirmer, J. An efficient polarization propagator approach to valence electron excitation spectra. *J. Phys. B* **1995**, *28*, 2299–2324.

(121) Frisch, M. J.; Trucks, G. W.; Schlegel, H. B.; Scuseria, G. E.; Robb, M. A.; Cheeseman, J. R.; Scalmani, G.; Barone, V.; Mennucci, B.; Petersson, G. A.; Nakatsuji, H.; Caricato, M.; Li, X.; Hratchian, H. P.; Izmaylov, A. F.; Bloino, J.; Zheng, G.; Sonnenberg, J. L.; Hada, M.; Ehara, M.; Toyota, K.; Fukuda, R.; Hasegawa, J.; Ishida, M.; Nakajima, T.; Honda, Y.; Kitao, O.; Nakai, H.; Vreven, T.; Montgomery, J. A.; Peralta, J. E.; Ogliaro, F.; Bearpark, M.; Heyd, J. J.; Brothers, E.; Kudin, K. N.; Staroverov, V. N.; Kobayashi, R.; Normand, J.; Raghavachari, K.; Rendell, A.; Burant, J. C.; Iyengar, S. S.; Tomasi, J.; Cossi, M.; Rega, N.; Millam, J. M.; Klene, M.; Knox, J. E.; Cross, J. B.; Bakken, V.; Adamo, C.; Jaramillo, J.; Gomperts, R.; Stratmann, R. E.; Yazyev, O.; Austin, A. J.; Cammi, R.; Pomelli, C.; Ochterski, J. W.; Martin, R. L.; Morokuma, K.; Zakrzewski, V. G.; Voth, G. A.; Salvador, P.; Dannenberg, J. J.; Dapprich, S.; Daniels, A. D.; Farkas,; Foresman, J. B.; Ortiz, J. V.; Cioslowski, J.; Fox, D. J. Gaussian 09, Revision A.02. 2009.

(122) Schäfer, A.; Huber, C.; Ahlrichs, R. Fully optimized contracted Gaussian basis sets of triple zeta valence quality for atoms Li to Kr. *J. Chem. Phys.* **1994**, *100*, 5829–5835.

(123) Farmanara, P.; Stert, V.; Radloff, W. Ultrafast internal conversion and fragmentation in electronically excited C2H4 and C2H3Cl molecules. *Chem. Phys. Lett.* **1998**, *288*, 518–522.

(124) Mestdagh, J. M.; Visticot, J. P.; Elhanine, M.; Soep, B. Prereactive evolution of monoalkenes excited in the 6 eV region. *J. Chem. Phys.* **2000**, *113*, 237–248.

(125) Stert, V.; Lippert, H.; Ritze, H. H.; Radloff, W. Femtosecond time-resolved dynamics of the electronically excited ethylene molecule. *Chem. Phys. Lett.* **2004**, *388*, 144–149.

(126) Kosma, K.; Trushin, S. A.; Fuss, W.; Schmid, W. E. Ultrafast dynamics and coherent oscillations in ethylene and ethylene-d4 excited at 162. *J. Phys. Chem. A* **2008**, *112*, 7514–7529.

(127) Schepp, O.; Baumann, A.; Wieland, M.; Azima, A.; Drescher, M. VUV-induced dynamics of the electronically excited C2D4 molecule in a single-color pump-probe experiment. *Chem. Phys. Lett. X* **2019**, *3*.

(128) Shao, Y.; Head-Gordon, M.; Krylov, A. I. The spin-flip approach within time-dependent density functional theory: Theory and applications to diradicals. *J. Chem. Phys.* **2003**, *118*, 4807–4818.

(129) Melnichuk, A.; Bartlett, R. J. Relaxed active space: Fixing tailored-CC with high order coupled cluster. II. *J. Chem. Phys.* **2014**, *140*, 064113.

(130) Mato, J.; Gordon, M. S. A general spin-complete spin-flip configuration interaction method. *Phys. Chem. Chem. Phys.* **2018**, *20*, 2615–2626.

(131) Buenker, R. J.; Bonačić-Koutecký, V.; Pogliani, L. Potential energy and dipole moment surfaces for simultaneous torsion and pyramidalization of ethylene in its lowest-lying singlet excited states: A CI study of the sudden polarization effect. *J. Chem. Phys.* **1980**, *73*, 1836–1849.

(132) Krawczyk, R. P.; Viel, A.; Manthe, U.; Domcke, W. Photoinduced dynamics of the valence states of ethene: A six-dimensional potential-energy surface of three electronic states with several conical intersections. *J. Chem. Phys.* **2003**, *119*, 1397–1411.

(133) Musiał, M.; Lupa, Ł.; Szopa, K.; Kucharski, S. A. Potential energy curves via double ionization potential calculations: Example of 1,2-diazene molecule. *Struct. Chem.* **2012**, *23*, 1377–1382.

(134) Mahapatra, U. S.; Chattopadhyay, S. Evaluation of the performance of single root multireference coupled cluster method for ground and excited states, and its application to geometry optimization. *J. Chem. Phys.* **2011**, *134*.

(135) Barbatti, M.; Sen, K. Effects of different initial condition samplings on photodynamics and spectrum of pyrrole. *Int. J. Quantum Chem.* **2016**, *116*, 762–771.

(136) Sylwester, A. P.; Dervan, P. B. Low-temperature matrix isolation of the 1,1-diazene H2NN. Electronic and infrared characterization. *J. Am. Chem. Soc.* **1984**, *106*, 4648–4650.

(137) Narten, A. H.; Levy, H. A. Liquid Water: Molecular Correlation Functions from X-Ray Diffraction. *J. Chem. Phys.* **1971**, *55*, 2263–2269.

# Graphical TOC Entry